© 2021. Published by The Company of Biologists Ltd | Development (2021) 148, dev199922. doi:10.1242/dev.199922

RESEARCH ARTICLE

KATNB1 is a master regulator of multiple katanin enzymes in male meiosis and haploid germ cell development

Jessica E. M Dunleavy[1,2,*], Anne E. O'Connor[1,2], Hidenobu Okuda[1], D. Jo Merriner[1,2] and Moira K. O'Bryan[2]

ABSTRACT

Katanin microtubule-severing enzymes are crucial executers of microtubule regulation. Here, we have created an allelic loss-of-function series of the katanin regulatory B-subunit KATNB1 in mice. We reveal that KATNB1 is the master regulator of all katanin enzymatic A-subunits during mammalian spermatogenesis, wherein it is required to maintain katanin A-subunit abundance. Our data shows that complete loss of KATNB1 from germ cells is incompatible with sperm production, and we reveal multiple new spermatogenesis functions for KATNB1, including essential roles in male meiosis, acrosome formation, sperm tail assembly, regulation of both the Sertoli and germ cell cytoskeletons during sperm nuclear remodelling, and maintenance of seminiferous epithelium integrity. Collectively, our findings reveal that katanins are able to differentially regulate almost all key microtubule-based structures during mammalian male germ cell development, through the complexing of one master controller, KATNB1, with a 'toolbox' of neofunctionalised katanin A-subunits.

KEY WORDS: Male fertility, Male infertility, Microtubules, Spermiogenesis, Acrosome, Axoneme, Meiotic spindle, Microtubule severing

INTRODUCTION

Since its discovery in 1991 (Vale, 1991), microtubule (MT) severing has emerged as a fundamental MT regulation mechanism, and the eponymous MT-severing enzyme, katanin, remains the most well-characterised executer of this function (McNally and Roll-Mecak, 2018). Katanin is typically described as being composed of the canonical 60 kDa catalytic (KATNA1; p60 or A-subunit) and 80 kDa regulatory (KATNB1; p80 or B-subunit) subunits. Two KATNA1 paralogues, KATNAL1 and KATNAL2, and one KATNB1 paralogue, KATNBL1, also exist in higher order species. The katanin A-subunits are members of the AAA superfamily ('ATPases associated with diverse cellular activities') (Frickey and Lupas, 2004), which utilise ATP hydrolysis to remodel target substrates. Katanin A-subunits specifically target the α/β-tubulin MT lattice. A katanin A-subunit hexamer threads the tubulin C-terminal tail through a central pore and, upon ATP hydrolysis, 'tugs' the tail thereby disrupting tubulin-tubulin contacts, removing the heterodimer from the lattice (Zehr et al., 2017; Zehr et al., 2020). Progressive heterodimer removal results in MT severing (Vemu et al., 2018) and achieves diverse outcomes, including MT disassembly, release of MTs from nucleation sites, and generation of short stable seeds for intracellular transport or MT amplification (reviewed by McNally and Roll-Mecak, 2018). Incomplete severing can conversely stabilise MTs through replacement of GDP-associated tubulin heterodimers with more stable GTP-associated forms (Vemu et al., 2018).

The katanin B-subunit, although not capable of severing per se, regulates katanin A-subunit stability (Grode and Rogers, 2015) and bioactivity (Hartman et al., 1998; McNally et al., 2000, 2006; McNally and McNally, 2011; Cheung et al., 2016; Joly et al., 2016) and targets the A-subunits to key cellular sites (Hartman et al., 1998; McNally et al., 2000; Srayko et al., 2000). This regulation is complex and context dependent, with B-subunits able to both enhance (Hartman et al., 1998; McNally et al., 2000; Grode and Rogers, 2015; Cheung et al., 2016) and inhibit (McNally et al., 2000; Cheung et al., 2016) A-subunit activity. Testament to the B-subunit's importance, in *Caenorhabditis elegans* the katanin A-subunit orthologue MEI-1 is incapable of MT severing in the absence of the B-subunit orthologue MEI-2 (McNally et al., 2006; Joly et al., 2016). In humans, sea urchins and *Drosophila*, katanin A-subunits can sever MTs independently of the B-subunit; however, their activity and MT affinity is significantly enhanced in its presence (Cheung et al., 2016; Hartman et al., 1998; McNally et al., 2000; Grode and Rogers, 2015).

Although a substantial body of work has been devoted to fundamental aspects of katanin-mediated MT severing, how these proteins contribute to complex mammalian biological systems and in scenarios wherein multiple katanin paralogues co-exist has received less attention. There is however, increasing evidence that the nervous system (e.g. Banks et al., 2018; Hu et al., 2014; Mishra-Gorur et al., 2014) and spermatogenesis (e.g. Dunleavy et al., 2017; O'Donnell et al., 2012; Smith et al., 2012) are particularly reliant on katanin proteins. Previously, we showed that spermatogenesis is crucially reliant on the A-subunits KATNAL1 and KATNAL2 (Dunleavy et al., 2017; Smith et al., 2012). Moreover, we showed that a hypomorphic point mutation in the B-subunit *Katnb1* results in spermatogenic abnormalities, but was compatible with the production of sperm, albeit infertile morphologically abnormal sperm (O'Donnell et al., 2012). Of note, there was a disconnect between the range and severity of spermatogenic phenotypes within the *Katnb1* hypomorphic mice, compared with the *Katnal1* and *Katnal2* mutant mouse lines (Dunleavy et al., 2017; Smith et al., 2012), indicating that the *Katnb1* hypomorphic mouse did not reflect the full extent of KATNB1 function. Consistent with this hypothesis, we subsequently showed that complete *Katnb1* ablation in mice resulted in embryonic lethality (Furtado et al., 2017).

Here, through a graded series of KATNB1 loss-of-function (LOF) mutations, we reveal that KATNB1 is essential for sperm

[1]School of Biological Sciences, Faculty of Science, Monash University, Clayton, VIC, 3800, Australia. [2]School of BioSciences, Faculty of Science, The University of Melbourne, Parkville, VIC, 3010, Australia.

*Author for correspondence (Jessica.dunleavy@unimelb.edu.au)

J.E.MD., 0000-0003-2009-0165; A.E.O., 0000-0001-9334-4256; H.O., 0000-0001-5953-2421; D.J.M., 0000-0003-3975-3205; M.K.O., 0000-0001-7298-4940

Handling Editor: Haruhiko Koseki
Received 7 July 2021; Accepted 16 November 2021

Development (2021) 148, dev199922. doi:10.1242/dev.199922

production, with essential roles in meiosis, acrosome formation, spermatid head shaping and flagella development. Our results establish KATNB1 as a master regulator of all three katanin A-subunits within the testis and highlight spermatogenesis as an exceptional tool for the study of gene duplication and neofunctionalisation events.

RESULTS

The KATNB1 LOF allelic series

To test the hypothesis that KATNB1 contributes to multiple facets of male germ cell development mediated by multiple katanin A-subunits, we created an allelic series of KATNB1 LOF mice ranging from wild-type to complete germ cell knockout (KO) models. This consisted of: (1) the *Katnb1* hypomorphic (*Katnb1*$^{Taily/Taily}$) mice which produce a partial LOF protein (O'Donnell et al., 2012); (2) compound heterozygous *Katnb1*$^{Taily/KO}$ mice, generated through inter-crossing of heterozygous *Katnb1* KO (*Katnb1*$^{KO/WT}$) and the Taily mutant mice; and (3) *Katnb1* germ cell KO (*Katnb1*$^{GCKO/GCKO}$) mice (Fig. 1, Table 1). *Katnb1*$^{KO/KO}$ mice die mid-gestation (Furtado et al., 2017). Similarly, a proportion of *Katnb1*$^{Taily/KO}$ mice die perinatally as a result of heart defects (Furtado et al., 2017), thus only males that survived to adulthood were analysed. Aside from the testicular phenotypes detailed below, these *Katnb1*$^{Taily/KO}$ adult males were superficially healthy. However, given the role of KATNB1 in brain development in humans, zebrafish and *Drosophila* (Hu et al., 2014; Mishra-Gorur et al., 2014), we anticipate extra-testicular defects. An analysis of these consequences was outside the scope of the current study.

In all three models, *Katnb1* mRNA expression was significantly reduced in purified spermatocytes compared with strain-specific controls (Fig. 1D). In *Katnb1*$^{Taily/Taily}$ spermatocytes, *Katnb1* mRNA was reduced by 35.2%, suggesting that the Taily point mutation negatively impacts mRNA stability. In *Katnb1*$^{Taily/KO}$, *Katnb1* mRNA was reduced by 59.3%, whereas in *Katnb1*$^{GCKO/GCKO}$ spermatocytes, it was reduced by 99.8% (Fig. 1D). Likewise, across all three lines KATNB1 protein was reduced (Fig. 1E). In *Katnb1*$^{Taily/Taily}$ and *Katnb1*$^{Taily/KO}$ testis lysates, KATNB1 was reduced by ∼82% and ∼93%, respectively. The greater reduction in KATNB1 protein compared with mRNA in these two models indicates that the Taily mutation negatively impacts mRNA and/or protein stability. Finally, in *Katnb1*$^{GCKO/GCKO}$ testis lysates, KATNB1 was reduced by ∼99% (Fig. 1E). We note that in this model, KATNB1 function will be intact within Sertoli cells.

KATNB1 has been shown to complex with each of the three katanin A-subunits by co-immunoprecipitation assays (e.g. Mishra-Gorur et al., 2014; Cheung et al., 2016; Rezabkova et al., 2017; Hartman et al., 1998; Srayko et al., 2000; McNally et al., 2000; McNally and McNally, 2011; Dunleavy et al., 2017), and emerging evidence from *Drosophila* suggests that these interactions stabilise, and thus maintain the abundance of, katanin A-subunits (Grode and Rogers, 2015). Accordingly, herein the KATNB1 reductions were associated with proportional and pronounced reductions in each of the three katanin A-subunits in the testis (Fig. 1F-H and summarised in Table 1) suggesting that mammalian KATNB1 also regulates the abundance of katanin catalytic subunits. Moreover, this suggests that the allelic series presented here is a graded loss of total katanin family function rather than KATNB1 in isolation.

The dramatic reduction in katanin A-subunit expression in *Katnb1*$^{GCKO/GCKO}$ testis lysates (Fig. 1G,H) suggests that within the testis all three A-subunits are predominantly found in the germ line, which comprises the bulk of the testis. This interpretation is confirmed by recent single-cell RNA-sequencing studies of the mouse and human testis transcriptome (Jung et al., 2019; Guo et al., 2018; Ernst et al., 2019; Wang et al., 2018). The mouse testis mRNA expression profiles for each of the katanin A-subunits are presented in Fig. S1.

Spermatogenic deficits scale with increasing severity of *Katnb1* depletion

All *Katnb1* LOF mice exhibited normal body weight (Fig. S2). As expected, adult testis weights were significantly decreased in mutants compared with controls, and positively correlated with KATNB1 functional competence (31.8% reduction in *Katnb1*$^{Taily/Taily}$, 49.8% in *Katnb1*$^{Taily/KO}$ and 71.5% in *Katnb1*$^{GCKO/GCKO}$; Fig. 2A). Testis daily sperm production (DSP) was significantly reduced in all mutants, compared with controls, and scaled with KATNB1 expression (59.9% reduction in *Katnb1*$^{Taily/Taily}$, 83.6% in *Katnb1*$^{Taily/KO}$ and 91.9% in *Katnb1*$^{GCKO/GCKO}$; Fig. 2B). Reflective of sperm numbers, the number of apoptotic germ cells was significantly increased in *Katnb1*$^{Taily/KO}$ and *Katnb1*$^{GCKO/GCKO}$ testes compared with their respective controls (Fig. S3A). The number of apoptotic cells in *Katnb1*$^{Taily/Taily}$ did not reach statistical significance above wild-type levels (Fig. S3A). The bulk of the apoptotic cells were spermatocytes undergoing meiosis I in stage XII and I seminiferous tubules (Fig. S3B), indicating that this is the first point in adult spermatogenesis at which KATNB1 plays a life-and-death role.

We previously showed that the reduced spermatogenic output observed in *Katnb1*$^{Taily/Taily}$ was principally due to spermatocytes stalling, then frequently dying, in anaphase and cytokinesis, resulting in fewer spermatids (O'Donnell et al., 2012). More subtle meiotic defects during metaphase were also observed, including increased meiotic spindle MT density, MTs projecting from spindle poles at a wider angle and increased spindle pole-to-pole length. This was followed by pronounced defects in spermatid ultrastructure (head shaping and flagella formation), and partial spermiation failure.

As detailed below and summarised in Table 1, in comparison with *Katnb1*$^{Taily/Taily}$, more severe and additional phenotypes were observed in *Katnb1*$^{Taily/KO}$ and *Katnb1*$^{GCKO/GCKO}$ testes and this resulted in the more dramatic spermatogenic output reductions described above. In addition to the defects seen in *Katnb1*$^{Taily/Taily}$ sections, numerous seminiferous tubules within *Katnb1*$^{Taily/KO}$ and *Katnb1*$^{GCKO/GCKO}$ contained multinucleated syncytia (symplasts) comprising round spermatids and, less frequently, Sertoli cells (Fig. 2D). We also observed prematurely sloughed spermatocytes and round spermatids in the lumen of *Katnb1*$^{Taily/KO}$ and *Katnb1*$^{GCKO/GCKO}$ seminiferous tubules and epididymides (Fig. 2D,E). These phenotypes were not observed in *Katnb1*$^{WT/WT}$ testis sections, and infrequently in *Katnb1*$^{Taily/Taily}$ (Fig. 2). These data suggest that KATNB1 is required to maintain intercellular germ-germ cell and germ-Sertoli adhesion. Although not directly tested herein, we predict that the collapse of Sertoli cells into symplasts is secondary to germ cell loss as this phenotype was seen in *Katnb1*$^{GCKO/GCKO}$ testes, in which Sertoli cell KATNB1 expression should remain intact. Of the spermatids that remained in the seminiferous epithelium, the vast majority became pyknotic by step 15 (stage IV) in *Katnb1*$^{Taily/KO}$ (Fig. 2D) and by step 13 (stage I) in *Katnb1*$^{GCKO/GCKO}$ (Figs 2D and 7B) mice.

Epididymal sperm content was significantly reduced in all of *Katnb1*$^{Taily/Taily}$, *Katnb1*$^{Taily/KO}$ and *Katnb1*$^{GCKO/GCKO}$ mice compared with controls (by 79.5%, 99.7% and 99.5%, respectively; Fig. 2C). These reductions were more severe than those for DSP, indicating a failure of spermatid release (spermiation). We previously showed

Development (2021) 148, dev199922. doi:10.1242/dev.199922

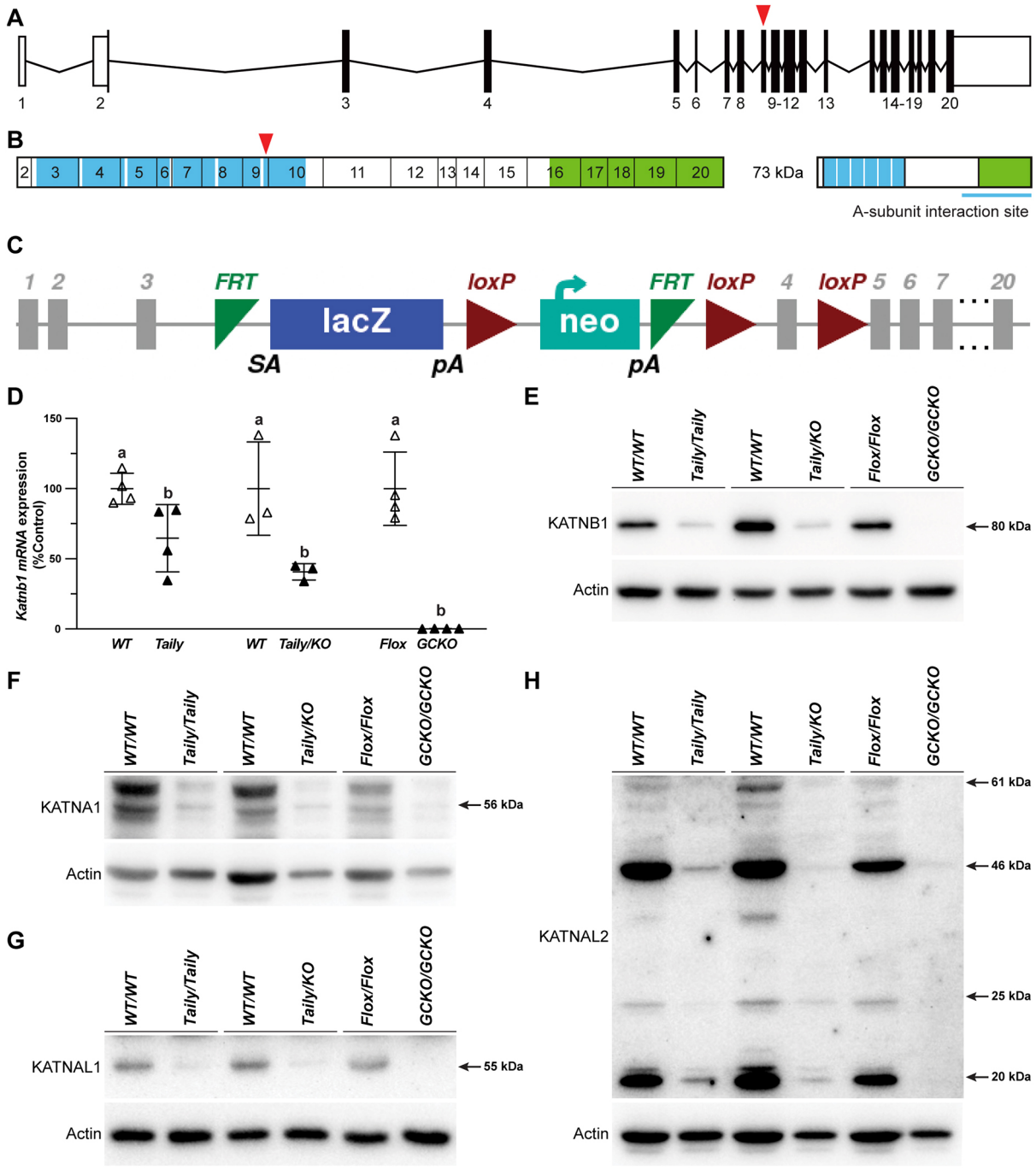

Fig. 1. KATNB1 LOF allelic series. (A,B) *Katnb1* gene (A), transcript and protein (B) schematics. WD40 repeats and the con80 domain are shown in blue and green, respectively. Red arrowheads indicate the Taily point mutation. (C) *Katnb1* KO-first conditional ready allele. The FRT-lacZ-loxP-Neo-FRT-loxP-*Katnb1* exon 4-loxP cassette was inserted into *Katnb1* intron 3. (D) qPCR analysis of *Katnb1* transcript levels in $Katnb1^{Taily/Taily}$, $Katnb1^{Taily/KO}$, and $Katnb1^{GCKO/GCKO}$ isolated spermatocytes relative to strain-specific controls (n=3-4/genotype). Data are normalised to *Ppia* and lines represent mean±s.d. Different lowercase letters indicate significantly different *P*-values compared with respective controls, calculated using an unpaired Student's *t*-test. Compared with respective controls, $P<0.05$ for $Katnb1^{Taily/Taily}$ and $Katnb1^{Taily/KO}$ and $P<0.0001$ for $Katnb1^{GCKO/GCKO}$. (E-H) Western blot analysis of KATNB1 (E), KATNA1 (F), KATNAL1 (G) and KATNAL2 (H) in whole-testis homogenates from $Katnb1^{Taily/Taily}$, $Katnb1^{Taily/KO}$, $Katnb1^{GCKO/GCKO}$ and respective control adult (>7 weeks of age) mice. Blots were re-probed with actin as a loading control.

such failures are visible in stage IX $Katnb1^{Taily/Taily}$ tubules and lead to a significant increase in spermatids being phagocytosed by Sertoli cells (O'Donnell et al., 2012).

KATNB1 has multiple essential roles in male meiosis

In $Katnb1^{Taily/Taily}$ testis sections, although some abnormal metaphase spermatocytes were observed (Fig. 3Ab,An, black arrowheads), for most chromosome alignment appeared overtly normal (Fig. 3Ab). Consistent with our previous findings, the most apparent $Katnb1^{Taily/Taily}$ metaphase defect was that chromosomes were more widely spaced compared with controls (Fig. 3Ag-Ah). In contrast, the majority of $Katnb1^{Taily/KO}$ and $Katnb1^{GCKO/GCKO}$ metaphase spermatocytes possessed lagging and/or misaligned chromosomes (Fig. 3Ac,Ad,Ao, black arrowheads). Metaphase

Development (2021) 148, dev199922. doi:10.1242/dev.199922

Table 1. Summary of spermatogenesis phenotypes in the *Katnb1* LOF allelic series

		Genotype			
		Katnb1$^{WT/WT}$	*Katnb1*$^{Taily/Taily}$	*Katnb1*$^{Taily/KO}$	*Katnb1*$^{GCKO/GCKO}$
***Katnb1* allele**	WT	++			
	Taily		++	+	
	KO			+	
	GCKO				++
KATNB1 expression	mRNA	++++++	++++*	++*	- (<0.25%) ****
	Protein	++++++	++	+	– (<2%)
A-subunit expression	KATNA1	++++++	++	+	+
	KATNAL1	++++++	++	+	+
	KATNAL2	++++++	++	+	+
Phenotypes	Body weight	++++++	++++++	++++++	++++++
Testis output	Testis weight	++++++	++++***	+++ ****	++****
	DSP	++++++	+++ ****	+ ****	+****
	ESC	++++++	+ ****	_ ****	_ ****
Origins of reduced spermatogenic output	Spermatocyte apoptosis	–	–	++***	+++ ***
	Sloughing of germ cells	–	+	++	++
	Pyknotic spermatids	–	–	+	++
	Spermiation failure	–	+	Not able to assess	Not able to assess
Meiotic phenotypes	Large/wide metaphase spindles	–	+	++	++
	Misaligned metaphase chromosomes	–	+	++	++
	Abnormal spindle architecture	–	Not assessed	+++ ***	+++ ***
	Stalled anaphase and telophase cells	–	+	++	++
	Uneven chromosome segregation	–	–	+	+
	Telekinesis failure (multi-nucleated spermatids)	–	+	+	+
Spermiogenesis phenotypes	Abnormal acrosome formation	–	–	+++ ****	+++++ ****
	Sperm tail defects	–	+++++	+++++	+++++
	Failure of manchette formation	–	–	+++++	++
	Failure of manchette movement	–	++++++	Not able to assess	++++++
	Excessive manchette elongation	–	++++++	Not able to assess	++++++
	Delayed manchette disassembly	–	++++++	Not able to assess	++++++
	Abnormal apical sperm head shaping	–	+	++++++	++

ESC, epididymal sperm content.

For each characteristic/phenotype relative manifestation, quantity or phenotype severity is shown with '++++++' representing 100% and '–' being 0%. *P<0.05, ***P<0.001, ****P<0.0001.

plates also frequently appeared wider than normal (Fig. 3Ai-Al). *Katnb1*$^{Taily/KO}$ and *Katnb1*$^{GCKO/GCKO}$ metaphase defects were associated with metaphase arrest and apoptosis in stage XII and I tubules, suggesting a causal relationship between metaphase defects and germ cell loss (Fig. 3Ap,As,At, red arrowheads, Fig. S3B,C).

Consistent with our previous data, *Katnb1*$^{Taily/Taily}$ meiotic defects were most apparent in anaphase and telophase of meiosis I. An abnormally high number of anaphase and telophase spermatocytes were present in stage XII seminiferous tubules, compared with controls (Fig. 3Ab,An, green arrowheads). In accordance, *Katnb1*$^{Taily/Taily}$ anaphase and telophase spermatocytes were frequently observed in stage I seminiferous tubules, long after meiosis should normally be completed (Fig. 3Ar, green arrowheads). Likewise, of *Katnb1*$^{Taily/KO}$ and *Katnb1*$^{GCKO/GCKO}$ spermatocytes that survived metaphase, many stalled in anaphase and telophase. In *Katnb1*$^{Taily/KO}$ and *Katnb1*$^{GCKO/GCKO}$ mice, these abnormalities were more severe than in *Katnb1*$^{Taily/Taily}$ with many pyknotic and caspase-positive anaphase and telophase spermatocytes present in stage I seminiferous tubules (Fig. 3As, At, blue arrowheads, Fig. S3B,C). Consistent with failures in cytokinesis, within all three lines double-nucleated spermatids (Fig. 3Ba-Be) were frequent. Furthermore, many *Katnb1*$^{Taily/KO}$ and *Katnb1*$^{GCKO/GCKO}$ round spermatid nuclei were frequently abnormally sized (some large, some small) suggestive of uneven chromosome segregation (Fig. 3Be-Bh). Abnormalities in spermatid nuclear size were occasionally seen in *Katnb1*$^{Taily/Taily}$ sections; however, these were relatively rare compared with *Katnb1*$^{Taily/KO}$ and *Katnb1*$^{GCKO/GCKO}$ sections.

To refine this analysis, *Katnb1*$^{Taily/KO}$ and *Katnb1*$^{GCKO/GCKO}$ metaphase spindle morphology was assessed in purified spermatocytes (Fig. 3C-J). Virtually all control metaphase cells contained a normal bipolar spindle (Fig. 3C,I). In *Katnb1*$^{Taily/KO}$ and *Katnb1*$^{GCKO/GCKO}$ spindles, however, approximately half contained spindle abnormalities (defined as multipolar and unipolar spindles, and bipolar spindles with misaligned spindle poles; 48% of *Katnb1*$^{Taily/KO}$ compared with 14% of *Katnb1*$^{WT/WT}$ and 52% in *Katnb1*$^{GCKO/GCKO}$ compared with 10% of *Katnb1*$^{Flox/Flox}$; Fig. 3H) and the proportion of bipolar spindles was significantly reduced (24% and 34% reduction in *Katnb1*$^{Taily/KO}$ and *Katnb1*$^{GCKO/GCKO}$, respectively; Fig. 3I). For both *Katnb1*$^{Taily/KO}$ and *Katnb1*$^{GCKO/GCKO}$ spermatocytes, the most common abnormalities were spindle pole misalignment, with the most severe instances displaying two poles on the same side of the cell (Fig. 3E,G,J), and multipolar spindles, with multiple centrosomes (Fig. 3D,F,J).

Development (2021) 148, dev199922. doi:10.1242/dev.199922

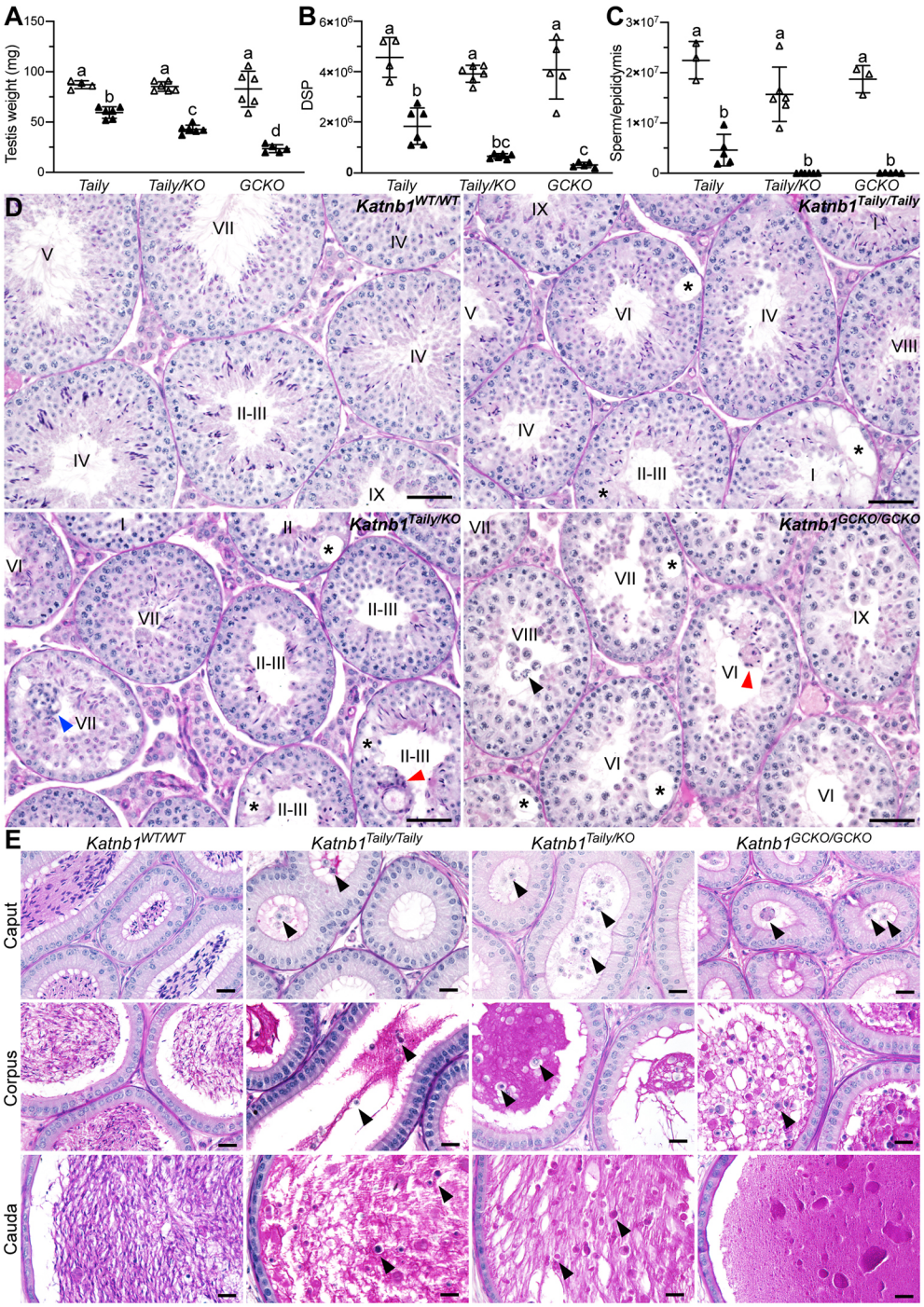

Fig. 2. Spermatogenic deficits scale with increasing severity of *Katnb1* depletion. (A-C) Testis weight (A), DSP (B) and epididymal sperm content (C) in *Katnb1*$^{Taily/Taily}$, *Katnb1*$^{Taily/KO}$ and *Katnb1*$^{GCKO/GCKO}$ mice (black triangles) compared with strain-specific controls (white triangles) ($n \geq 3$/genotype). Lines represent mean±s.d. Different lowercase letters indicate significantly different *P*-values, calculated using a one-way ANOVA. In A, compared with respective controls $P<0.001$ for b, $P<0.0001$ for c and d; compared with c $P<0.05$ for b and d; $P<0.0001$ for b compared with d. In B, compared with respective controls $P<0.0001$ for all KATNB1 LOF genotypes; $P<0.05$ for *Katnb1*$^{Taily/Taily}$ compared with *Katnb1*$^{GCKO/GCKO}$. In C, compared with respective controls $P<0.0001$ for all *Katnb1* mutant genotypes. (D,E) PAS-stained testis (D) and epididymis (E) sections. Asterisks indicate areas of seminiferous epithelium with vacuoles or devoid of germ cells. Red and blue arrowheads indicate multinucleated symplasts of germ and Sertoli cells, respectively. Black arrowheads indicate prematurely sloughed spermatocytes and spermatids. Roman numerals indicate seminiferous tubule stages in D. Scale bars: 50 µm (D); 20 µm (E).

KATNB1 complexes with all three katanin A-subunits during male meiosis

To identify the specific katanin A-subunit(s) mediating KATNB1 meiosis functions, we defined the localisation of KATNB1-KATNA1, KATNB1-KATNAL1 and KATNB1-KATNAL2 complexes in purified spermatocytes using *in situ* proximity ligation assays (PLAs) (Fig. 4, Fig. S4). For KATNB1-KATNA1 compared with other KATNB1 complexes, a relatively small number of complexes were observed (Fig. 4A, Fig. S4A). In prophase, KATNB1-KATNA1 complexes were typically in close proximity to cytoplasmic MTs. In metaphase and early anaphase, the few KATNB1-KATNA1 complexes present localised to MTs near the plasma membrane (Fig. 4A, Fig. S4A), suggesting localisation at astral spindle fibres. KATNB1-KATNA1 complexes, however, were absent from the spindle poles, interpolar fibres and kinetochore fibres.

KATNB1-KATNAL1 complexes were the most abundant of all the KATNB1 complexes during each meiotic phase (Fig. 4B, Fig. S4B). During prophase, they localised to MTs throughout the cytoplasm (Fig. 4B, Fig. S4B). In metaphase and anaphase cells, most colocalised with astral spindle fibres. Occasionally, complexes were associated with interpolar and kinetochore spindle MTs (Fig. 4B, Fig. S4B). KATNB1-KATNAL1 complexes were not observed at the spindle poles (Fig. 4B, Fig. S4B).

KATNB1-KATNAL2 complexes were present in prophase I. However, consistent with the absence of a meiosis phenotype in

Development (2021) 148, dev199922. doi:10.1242/dev.199922

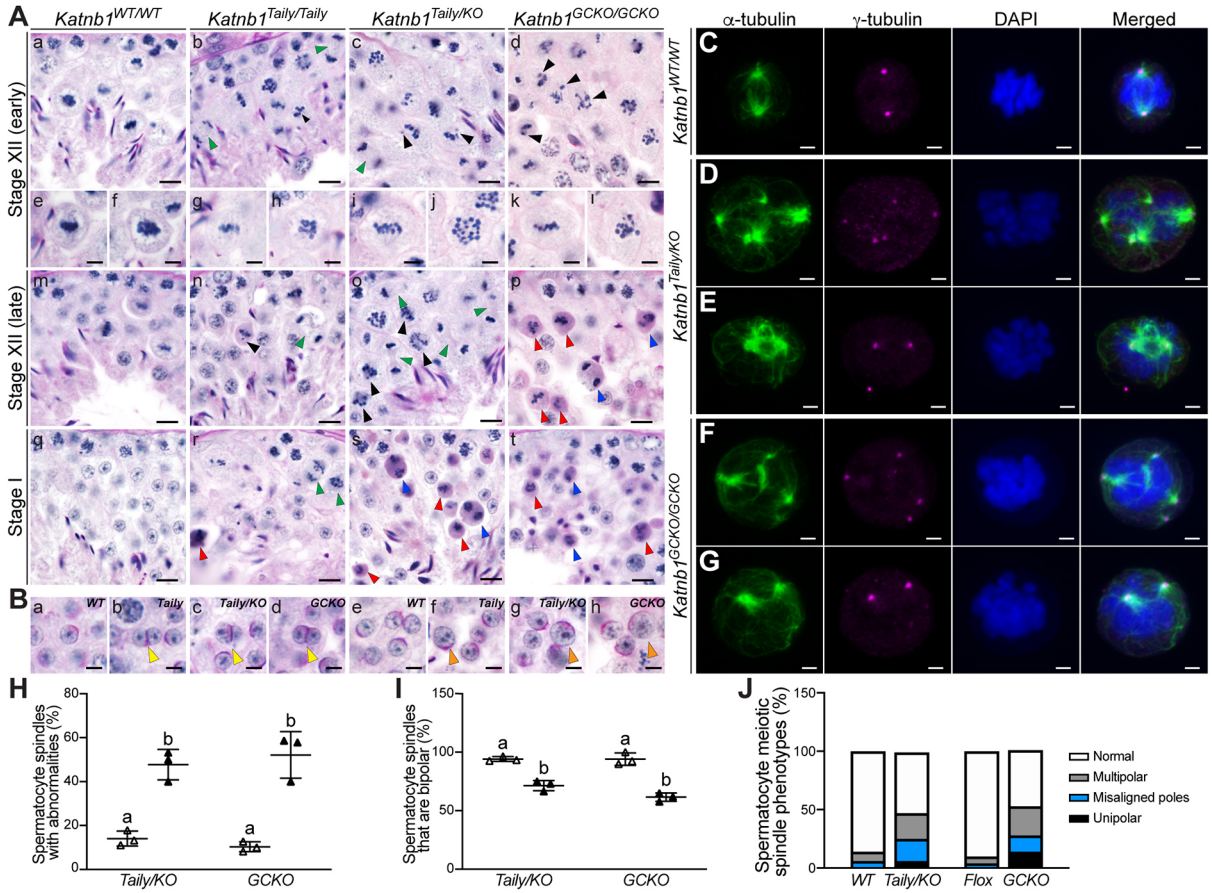

Fig. 3. KATNB1 has multiple essential roles in male meiosis. (Aa-At) PAS-stained testis sections revealed abnormal meiosis in KATNB1 LOF mice. Black arrowheads indicate metaphase spermatocytes with lagging and/or misaligned chromosomes. Green arrowheads indicate anaphase and telophase cells. Red arrowheads indicate pyknotic metaphase cells. Blue arrowheads indicate pyknotic anaphase cells. (Ba-Bh) KATNB1 LOF round spermatids had phenotypes consistent with abnormal meiosis. Yellow arrowheads indicate binucleated round spermatids. Orange arrowheads indicate abnormally sized round spermatid nuclei. Scale bars: 10 µm (Aa-Ad,Am-At); 5 µm (Ae-Al,Ba-Bh). (C-G) Isolated *Katnb1*$^{WT/WT}$, *Katnb1*$^{Taily/KO}$ and *Katnb1*$^{GCKO/GCKO}$ metaphase spermatocytes immunolabelled for spindle MTs with an α-tubulin antibody (green), for centrioles with a γ-tubulin antibody (magenta) and for DNA with DAPI (blue). Images represent *z*-stacks presented as 2D maximum intensity projections. Scale bars: 2 µm. (H,I) Percentage of metaphase spermatocyte spindles with abnormal architecture (H) (defined as multipolar and unipolar spindles, and bipolar spindles with misaligned spindle poles) and percentage of metaphase spermatocyte spindles that were bipolar (I) in *Katnb1*$^{Taily/KO}$ and *Katnb1*$^{GCKO/GCKO}$ (black triangles) compared with respective controls (white triangles) (*n*=3/genotype, and for each animal 10-40 spindles were assessed). Lines represent mean±s.d. and different lowercase letters indicate significantly different *P*-values, calculated using a one-way ANOVA. Compared with respective controls, in H $P<0.01$ for *Katnb1*$^{Taily/KO}$ and $P<0.001$ for *Katnb1*$^{GCKO/GCKO}$ and in I $P=0.0005$ for *Katnb1*$^{Taily/KO}$ and $P<0.0001$ for *Katnb1*$^{GCKO/GCKO}$. (J) Average percentage of each spermatocyte spindle phenotype assessed for H.

Katnal2 mutant mice (Dunleavy et al., 2017), KATNB1-KATNAL2 complexes were not overtly associated with MTs (Fig. 4C, Fig. S4C). Likewise, in subsequent phases, KATNB1-KATNAL2 complexes did not colocalise with the spindle poles, kinetochore or interpolar MTs. Numerous KATNB1-KATNAL2 complexes were, however, consistently associated with astral spindle fibres (Fig. 4C, Fig. S4C).

Consistent with our PLA data, assessment of total KATNB1 protein localisation in wild-type spermatocytes revealed that KATNB1 was present throughout meiosis (Fig. 4D). During prometaphase, metaphase and anaphase, KATNB1 localised to astral, interpolar and kinetochore spindle fibres, with relative KATNB1 abundance at each dramatically upregulated during metaphase (Fig. 4D). KATNB1 was most abundant at kinetochore fibres (Fig. 4D), in contrast to the distribution patterns of the KATNB1-based katanin complexes, which were all most abundant at astral spindle fibres (Fig. 4A-C, Fig. S4). Consistent with our PLA data, however, KATNB1 was not enriched at the spindle poles. In telophase and cytokinesis, KATNB1 abundance decreased (Fig. 4D). During telophase, distinct KATNB1 foci localised at interpolar MTs, in addition to MTs encasing the chromosomes (Fig. 4D). In cytokinesis, a few KATNB1 foci remained localised to the midbody MTs (Fig. 4D).

The role of KATNB1 in spermiogenesis

Despite the meiotic defects, all *Katnb1* mutant lines produced round spermatids. KATNB1 LOF, however, led to multiple defects in spermiogenesis, the process by which spermatids differentiate into highly polarised spermatozoa, and phenotype severity differed across the allelic series.

Acrosome formation requires KATNB1

In *Katnb1*$^{Taily/Taily}$ spermatids, formation of the acrosome, an enzymatic apical nuclear cap required for fertilisation, was comparable to that of wild-type littermates. By contrast in *Katnb1*$^{Taily/KO}$ and *Katnb1*$^{GCKO/GCKO}$ abnormalities were observed throughout acrosome biogenesis (Fig. 5A). Defects were first seen in the Golgi phase of acrosome development in a small subset of

Development (2021) 148, dev199922. doi:10.1242/dev.199922

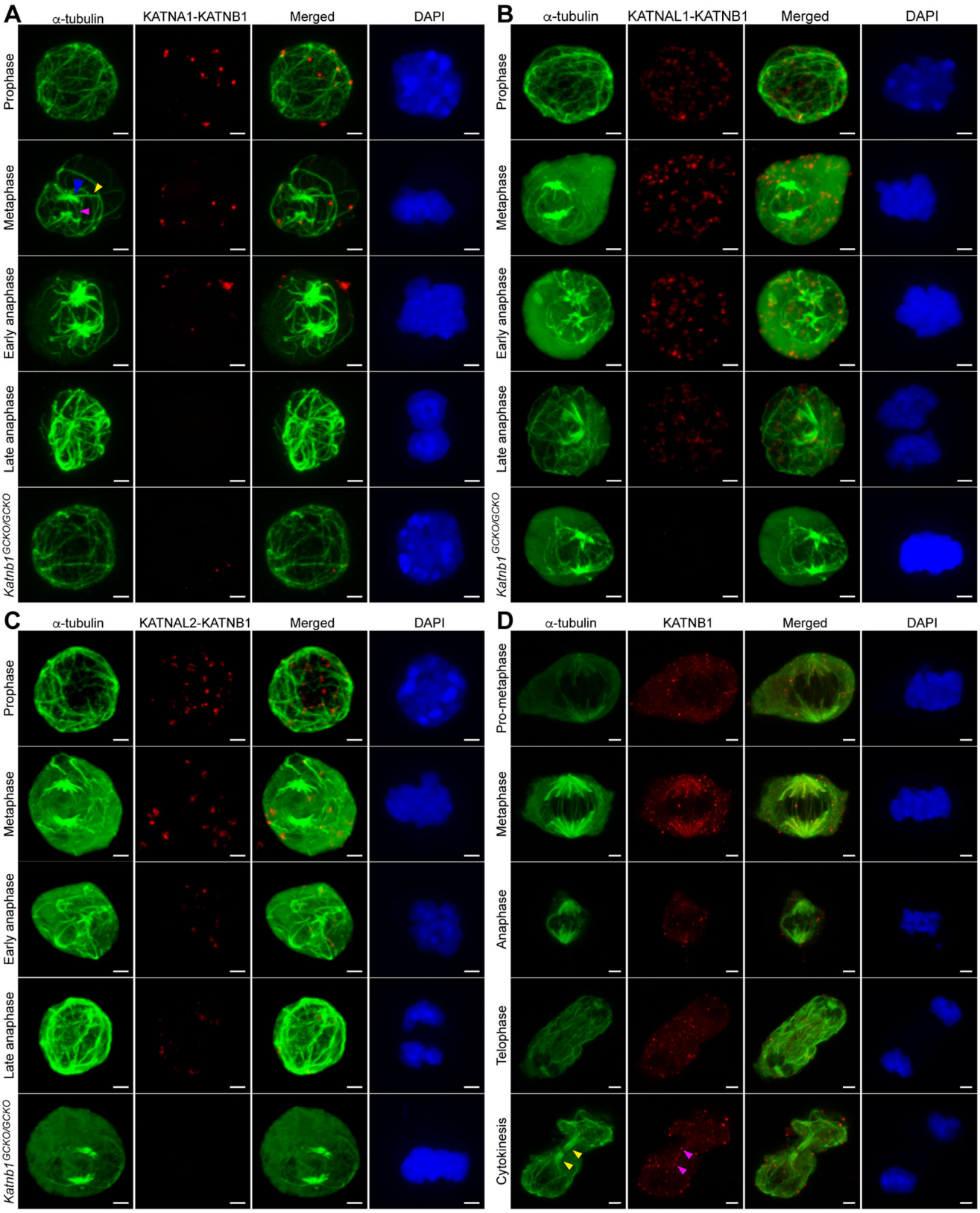

Fig. 4. KATNB1 complexes with all three katanin A-subunits during male meiosis. (A-C) *In situ* PLAs using antibodies directed against KATNA1 and KATNB1 (A), KATNAL1 and KATNB1 (B), and KATNAL2 and KATNB1 (C) in isolated *Katnb1*$^{Flox/Flox}$ spermatocytes. Assay specificity was shown by parallel staining of *Katnb1*$^{GCKO/GCKO}$ spermatocytes. For each assay, spermatocytes from *n*=3 *Katnb1*$^{Flox/Flox}$ mice and from *n*=1 *Katnb1*$^{GCKO/GCKO}$ mouse were assessed. Subgroups of images from each *z*-stack are presented in Fig. S4 for more precise localisation. Examples of kinetochore, interpolar and astral spindle fibres are indicated by blue, pink and yellow arrowheads, respectively. (D) KATNB1 immunolabelling (red) in isolated mouse spermatocytes. Yellow arrowheads indicate midbody MTs and pink arrowheads indicate KATNB1 puncta localised to the midbody. In A-D, MTs were stained with α-tubulin (green) and DNA with DAPI (blue). Images represent *z*-stacks presented as 2D maximum intensity projections. Scale bars: 2 µm.

Development (2021) 148, dev199922. doi:10.1242/dev.199922

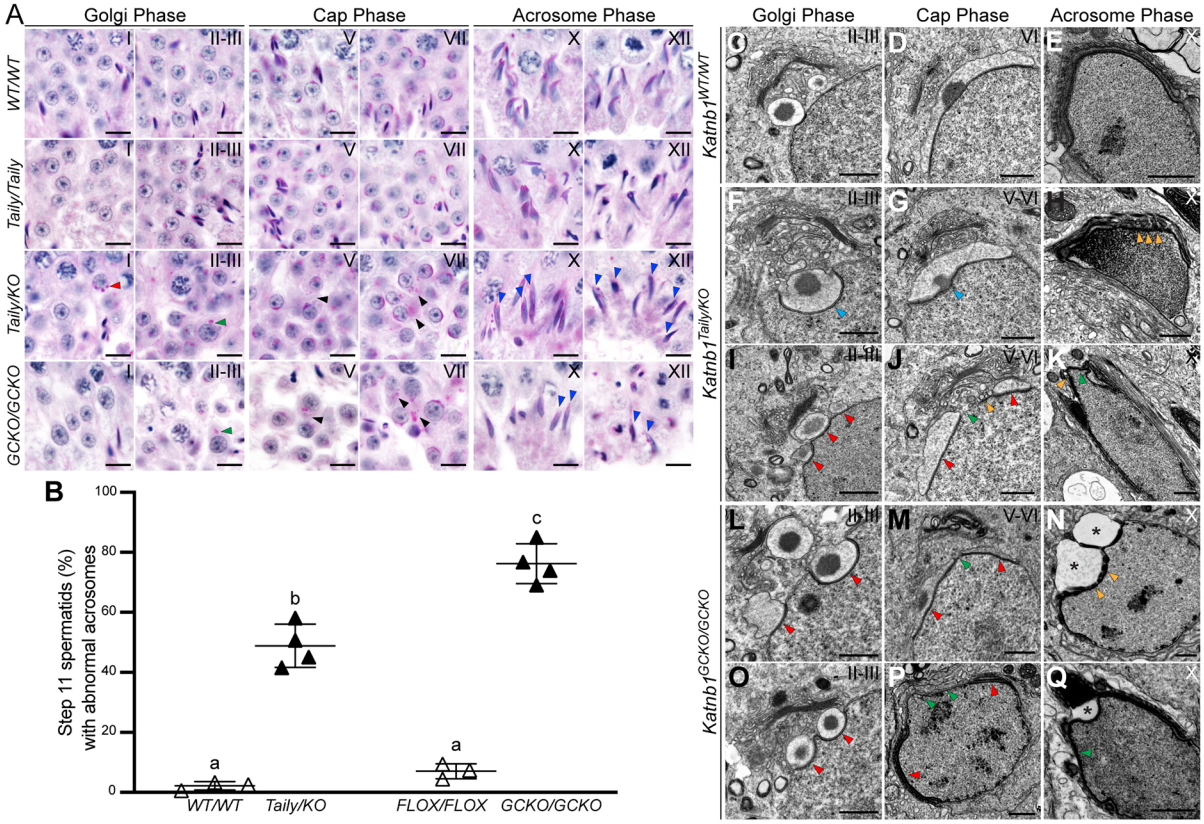

Fig. 5. Acrosome formation requires KATNB1 in mouse spermatids. (A) PAS-stained testis sections revealed multiple *Katnb1*$^{Taily/KO}$ and *Katnb1*$^{GCKO/GCKO}$ acrosome formation defects. Progressive steps of acrosome formation are shown left to right. Red arrowhead indicates more than one proacrosomal vesicle attaching to the nucleus. Green arrowheads indicate pro-acrosomal vesicles that failed to attach at the appropriate time. Black arrowheads indicate ectopic PAS-positive vesicles abnormally dispersed in round spermatid cytoplasm. Blue arrowheads indicate abnormal gaps and fragmentation of elongated spermatid acrosomes. Scale bars: 10 µm. (B) Percentage of step 11 spermatids in PAS-stained testis sections with acrosome abnormalities in *Katnb1*$^{Taily/KO}$ and *Katnb1*$^{GCKO/GCKO}$ (black triangles) compared with respective controls (white triangles) ($n \geq 3$/genotype, and for each animal all step 11 spermatids in ≥3 stage XI seminiferous tubules were assessed). Lines represent mean±s.d. Different lowercase letters indicate significantly different *P*-values calculated using a one-way ANOVA. Compared with respective controls $P<0.0001$ for b and c; $P<0.001$ for b compared with c. (C-Q) TEM of *Katnb1*$^{WT/WT}$, *Katnb1*$^{Taily/KO}$ and *Katnb1*$^{GCKO/GCKO}$ acrosome ultrastructure. Blue arrowheads indicate abnormal nuclear membrane deformation. Red arrowheads indicate supernumerary sites of acrosome formation. Green arrowheads indicate apical nuclear membrane abnormally devoid of acrosome. Orange arrowheads indicate numerous small unfused acrosomal vesicles docked at the nuclear membrane/fragmentation of the acrosome. Asterisks indicate abnormal large vacuoles within the acrosome. Scale bars: 1 µm. In A-Q, seminiferous tubule stage is indicated in the top right-hand corner.

Katnb1$^{Taily/KO}$ and *Katnb1*$^{GCKO/GCKO}$ round spermatids wherein more than the usual single proacrosomal vesicle attached to the nucleus (Fig. 5A, red arrowhead). Furthermore, in a small number of step 2-3 spermatids the proacrosomal vesicle(s) was located close to the nuclear membrane but appeared not to fuse with it (Fig. 5A, green arrowheads). In the subsequent cap phase, numerous Periodic acid-Schiff's (PAS)-positive vesicles were scattered throughout the cytoplasm of *Katnb1*$^{Taily/KO}$ and *Katnb1*$^{GCKO/GCKO}$ spermatids, indicative of defects in vesicle transport or fusion onto the nuclear membrane (Fig. 5A, black arrowheads). As spermiogenesis progressed, defects became more severe, ranging from gaps in the acrosomal cap, to only a few small acrosomal vesicles being associated with the nucleus indicative of an almost complete failure of acrosome vesicle attachment, fusion and migration (Fig. 5A, blue arrowheads). Quantification of these defects in PAS-stained seminiferous tubule cross-sections revealed that 49% of step 11 *Katnb1*$^{Taily/KO}$ spermatids had detectable acrosome abnormalities, compared with 2% in *Katnb1*$^{WT/WT}$ (Fig. 5B). In *Katnb1*$^{GCKO/GCKO}$, this phenotype was significantly more pronounced, with acrosome abnormalities in 76% of step 11 spermatids, compared with 7% in *Katnb1*$^{Flox/Flox}$ (Fig. 5B).

Transmission electron microscopy (TEM) confirmed the high frequency of abnormal acrosome formation in KATNB1-deficient spermatids (Fig. 5C-Q). During wild-type acrosome formation, a single large pro-acrosomal vesicle attaches to the acroplaxome (sub-acrosomal layer also called perinuclear theca; Fig. 5C) and is progressively enlarged (Fig. 5D) by vesicles derived from the Golgi apparatus (Golgi and cap phase/steps 2-7; Oko and Sutovsky, 2009) and the endocytic pathway (cap phase/step 4 onwards; Berruti and Paiardi, 2015; Berruti et al., 2010; Gioria et al., 2017) to eventually cover the spermatid's apical nuclear half (Fig. 5E). A subset of *Katnb1*$^{Taily/KO}$ and *Katnb1*$^{GCKO/GCKO}$ spermatids instead had multiple proacrosomal vesicles attached to the acroplaxome in steps 2-3 (Fig. 5I,L,O, red arrowheads), which led to multiple distinct acrosomal compartments forming (Fig. 5J,M,P, red arrowheads). In the cap phase, many small and distinct acrosomal vesicles were often docked at the nucleus, but failed to fuse with existing acrosomal compartments (Fig. 5J, orange arrowhead). In the subsequent acrosome phase, the observation of many distinct acrosomal vesicles docked at the nucleus (Fig. 5H,K,N, orange arrowheads) became more common suggesting acrosome fragmentation, in addition to a vesicle fusion failure. Segments of

Development (2021) 148, dev199922. doi:10.1242/dev.199922

the apical nuclear surface devoid of acrosome were often seen in cap and acrosome phase mutant spermatids but never in wild type (Fig. 5, green arrowheads). Within mutant cells, the acroplaxome formed (Fig. 5F-Q); however, it was typically only underneath sites of acrosome vesicle attachment, consistent with data suggesting that pro-acrosomal vesicles deliver acroplaxome components (Oko and Sutovsky, 2009). Nuclear deformations, whereby the nuclear surface appeared concave at the site of acrosome biogenesis, were frequent, suggesting loss of nucleoskeleton integrity (e.g. Fig. 5F,G, blue arrowheads).

Sperm tail formation in KATNB1 LOF is characterised by ectopic vesicles

Previously, we showed that *Katnb1*$^{Taily/Taily}$ mice produce sperm tails; however, key flagella components were frequently missing and motility was compromised (O'Donnell et al., 2012). Consistent with this, sperm flagella formed in *Katnb1*$^{Taily/KO}$ and *Katnb1*$^{GCKO/GCKO}$ mutants (Fig. 6A-D).

Sperm morphology in all KATNB1-deficient strains was abnormal (Fig. 6E). Defects in *Katnb1*$^{Taily/Taily}$ sperm included abnormally shaped heads (discussed below), in addition to decapitated and incorrectly reticulated heads, and acephalic tails (Fig. 6E), consistent with a weak head-tail coupling apparatus (HTCA). Assessment of the few *Katnb1*$^{Taily/KO}$ and *Katnb1*$^{GCKO/GCKO}$ epididymal sperm revealed increased severity of HTCA compromise with approximately half being decapitated (Fig. 6E). Most *Katnb1*$^{Taily/KO}$ and *Katnb1*$^{GCKO/GCKO}$ sperm tails were coiled, typically at the mid-piece (Fig. 6E). Within all three lines, a subset of sperm had mitochondrial sheath defects, with a complete lack of mitochondria in some, reminiscent of *Katnal2* mutant sperm (Dunleavy et al., 2017), and abnormal mid-piece thickness in others (Fig. 6E).

Flagella ultrastructure was assessed by TEM (Fig. 6F-V). Owing to insufficient epididymal sperm numbers, for *Katnb1*$^{Taily/KO}$ and *Katnb1*$^{GCKO/GCKO}$ these analyses were restricted to developing spermatid flagella within the testis, whereas for *Katnb1*$^{Taily/Taily}$ mature epididymal sperm were assessed. For all three lines, most flagella exhibited a superficially normal 9+2 MT axoneme (Fig. 6), suggesting that axoneme MTs, especially the central pair, are less sensitive to KATNB1 loss on the current C57BL/6 background compared with the CBA background we previously used to characterise the *Katnb1* Taily mutation (O'Donnell et al., 2012). Within a small subset of *Katnb1*$^{Taily/KO}$ spermatid flagella, excess and disorganised MT doublets were observed, a phenotype which, although infrequent, was never observed in controls (Fig. 6L,M).

The most common KATNB1 LOF flagella phenotype was the presence of ectopic vesicles (Fig. 6, red arrowheads). Within developing *Katnb1*$^{Taily/KO}$ and *Katnb1*$^{GCKO/GCKO}$ flagella, these vesicles were typically associated with axoneme MT doublets and ranged in size from ∼500 nm to larger than the axoneme itself (Fig. 6J-L,N, red arrowheads). Such vesicles were never observed in control samples (Fig. 6I). Assessment of *Katnb1*$^{Taily/Taily}$ epididymal sperm revealed that these vesicles persisted in the mid-piece (wherein they were most abundant), and in the principal piece, after sperm tail formation (Fig. 6H,P,R,T, red arrowheads). They were typically no longer associated with the axoneme but rather between adjacent mitochondria, between mitochondria and the outer dense fibres (ODFs), between the ODFs and the fibrous sheath, or between the transverse ribs of the fibrous sheath. Consistent with the mid-piece defects seen by light microscopy, mitochondria in *Katnb1*$^{Taily/Taily}$ sperm were improperly loaded onto the sperm tail and lacked the compact helical arrangement characteristic of wild-type mitochondria (Fig. 6P,T). Finally, within *Katnb1*$^{Taily/Taily}$ epididymal sperm samples, numerous degenerating sperm tails were observed (Fig. 6U,V), indicative of cell death or compromised integrity of the sperm tail itself.

KATNB1 has both Sertoli- and germ cell-specific roles in sperm head shaping

The manchette is a transient MT-based structure that shapes the sperm head's distal half and serves as an intracellular transport platform (Dunleavy et al., 2019a; Pleuger et al., 2020). In wild-type spermatids, manchette MTs appear in step 8 (marked by α-tubulin in Fig. 7B, Fig. S5), attaching via their plus ends [marked by CLIP170 (CLIP1); Fig. S5] to a perinuclear ring. Manchette MT minus ends project distally, towards the basal body and the cytoplasmic lobes (Fig. 7C, Fig. S5). As spermiogenesis continues, the manchette moves distally, and the perinuclear ring progressively constricts thus mechanically sculpting the sperm head's distal half (Fig. 7B). It is then disassembled at step 14 (Fig. 7B).

Katnb1$^{Taily/Taily}$ manchette biogenesis initiated appropriately at step 8. However, *Katnb1*$^{Taily/Taily}$ manchettes failed to migrate distally in subsequent steps (Fig. 7B, Fig. S5). By contrast, perinuclear ring constriction continued in a manner similar to wild type (Fig. 7B), with the net effect that *Katnb1*$^{Taily/Taily}$ spermatid nuclei were abnormally constricted leading to a 'knobby-head' phenotype (Fig. 7A). In addition, *Katnb1*$^{Taily/Taily}$ spermatid nuclei were abnormally elongated distal to the perinuclear ring and manchette disassembly was delayed (Fig. 7B).

Within many *Katnb1*$^{GCKO/GCKO}$ elongating spermatids, a similar 'knobby-head' and failed manchette migration phenotype was observed (Fig. 7A,B). The vast majority of step 13 *Katnb1*$^{GCKO/GCKO}$ nuclei (stage I), however, became pyknotic, indicating additional compromise to cell viability (Fig. 7B). *Katnb1*$^{GCKO/GCKO}$ spermatid cytoplasm became enriched with knot-like MT structures and typical manchettes were no longer observed (Fig. 7B). This suggests complete collapse of the manchette MT array followed by cell death. Consistent with this, staining of purified elongating spermatids for α-tubulin as a marker of the manchette and CLIP170 as a marker of the perinuclear ring revealed that although manchettes formed they often collapsed at the base of the sperm head, particularly in the final steps of elongation (Fig. S5, magenta arrowhead). In a separate subset of *Katnb1*$^{GCKO/GCKO}$ spermatids, an alternative phenotype was seen, wherein spermatid nuclei failed to elongate and there was a complete lack of manchette formation (Fig. 7A,B, green arrowheads). TEM confirmed these observations (Fig. 7C).

Strikingly, in contrast to *Katnb1*$^{Taily/Taily}$ and *Katnb1*$^{GCKO/GCKO}$, *Katnb1*$^{Taily/KO}$ elongated spermatids exhibited a 'curved edge blade-shaped' head (Fig. 7A, blue arrowheads). This reveals KATNB1 is also crucial for defining the shape of the apical half of sperm head via the Sertoli cells that envelope spermatids. In *Katnb1*$^{Taily/KO}$ mutants, which exhibit a deficit in Sertoli and germ cell KATNB1 content, MTs were enriched around step 8 spermatid nuclei (stage VIII), yet the typical manchette structure failed to form. Instead, MTs encased the entire length of the nucleus, rather than just the distal half (Fig. 7B). In other cells, MTs appeared to be enriched on only one aspect/side (Fig. 7B). This observation was confirmed in isolated spermatids immunolabelled for α-tubulin (MT marker) and PNA (acrosome marker), wherein MTs overlapped the acrosome (Fig. S6A).

TEM revealed that in *Katnb1*$^{Taily/KO}$ elongating spermatids, although MTs consistent with those of the manchette formed,

Development (2021) 148, dev199922. doi:10.1242/dev.199922

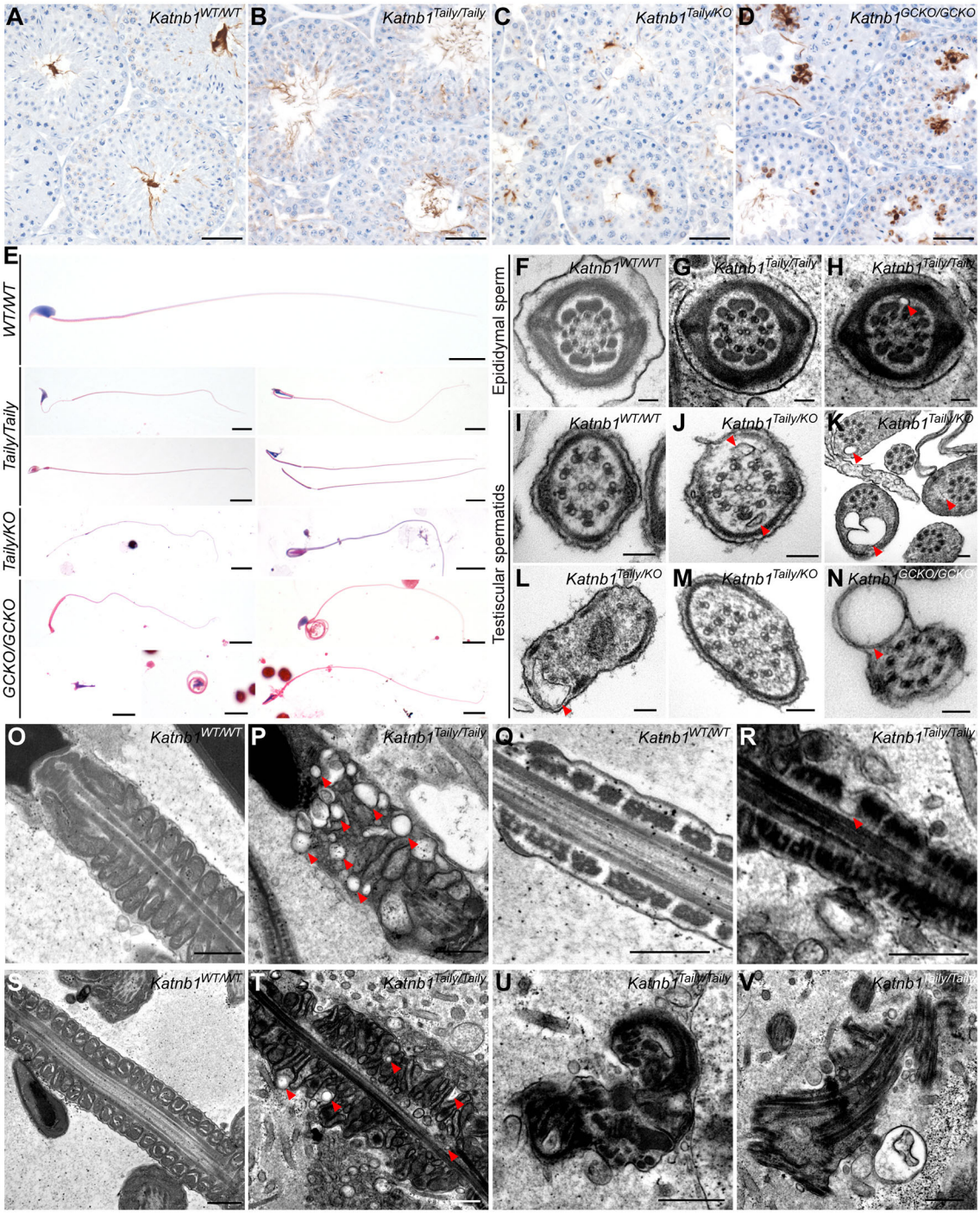

Fig. 6. KATNB1 LOF sperm tail formation is characterised by ectopic vesicles. (A-D) Testis sections immunolabelled for sperm tails with acetylated tubulin in *Katnb1*$^{WT/WT}$ (A), *Katnb1*$^{Taily/Taily}$ (B), *Katnb1*$^{Taily/KO}$ (C) and *Katnb1*$^{GCKO/GCKO}$ (D) mice. (E) Cauda epididymal sperm morphology in KATNB1 LOF mice. (F-V) TEM images of flagella ultrastructure in KATNB1 LOF mice. *Katnb1*$^{Taily/KO}$ and *Katnb1*$^{GCKO/GCKO}$ produced too few epididymal sperm for TEM, and as such for these lines developing spermatid flagella within the testis are shown, whereas epididymal sperm are shown for *Katnb1*$^{Taily/Taily}$. Because of this, the ODFs and fibrous sheath should not be compared in I-N as they are still being formed. Red arrowheads indicate ectopic vesicles. Scale bars: 50 µm (A-D); 10 µm (E); 0.1 µm (F-N); 0.5 µm (O-V).

perinuclear rings were absent, flimsy or only ectopic fragments were seen (Fig. 7C, Fig. S6B, red arrowheads). *Katnb1*$^{Taily/KO}$ manchette-like MTs were often oriented incorrectly (Fig. S6B, blue arrowheads), ectopically extended in a supranuclear location (Fig. 7C, blue arrowheads) and showed no, or minimal, association with the nucleus. CLIP170 immunolabelling confirmed that *Katnb1*$^{Taily/KO}$ spermatid MT plus ends did not form a discernible perinuclear ring structure (Fig. S5). The plus ends of manchette-like MTs in *Katnb1*$^{Taily/KO}$ were instead ectopically oriented and/or located and were arranged in small clusters instead of encircling the nucleus (Fig. S5, orange arrowhead). These data reveal that a balance between Sertoli and germ cell MT-based structures, and presumably the mechanical forces applied by the Sertoli cells on the apical pole of elongating spermatids, is required for positioning the

Development (2021) 148, dev199922. doi:10.1242/dev.199922

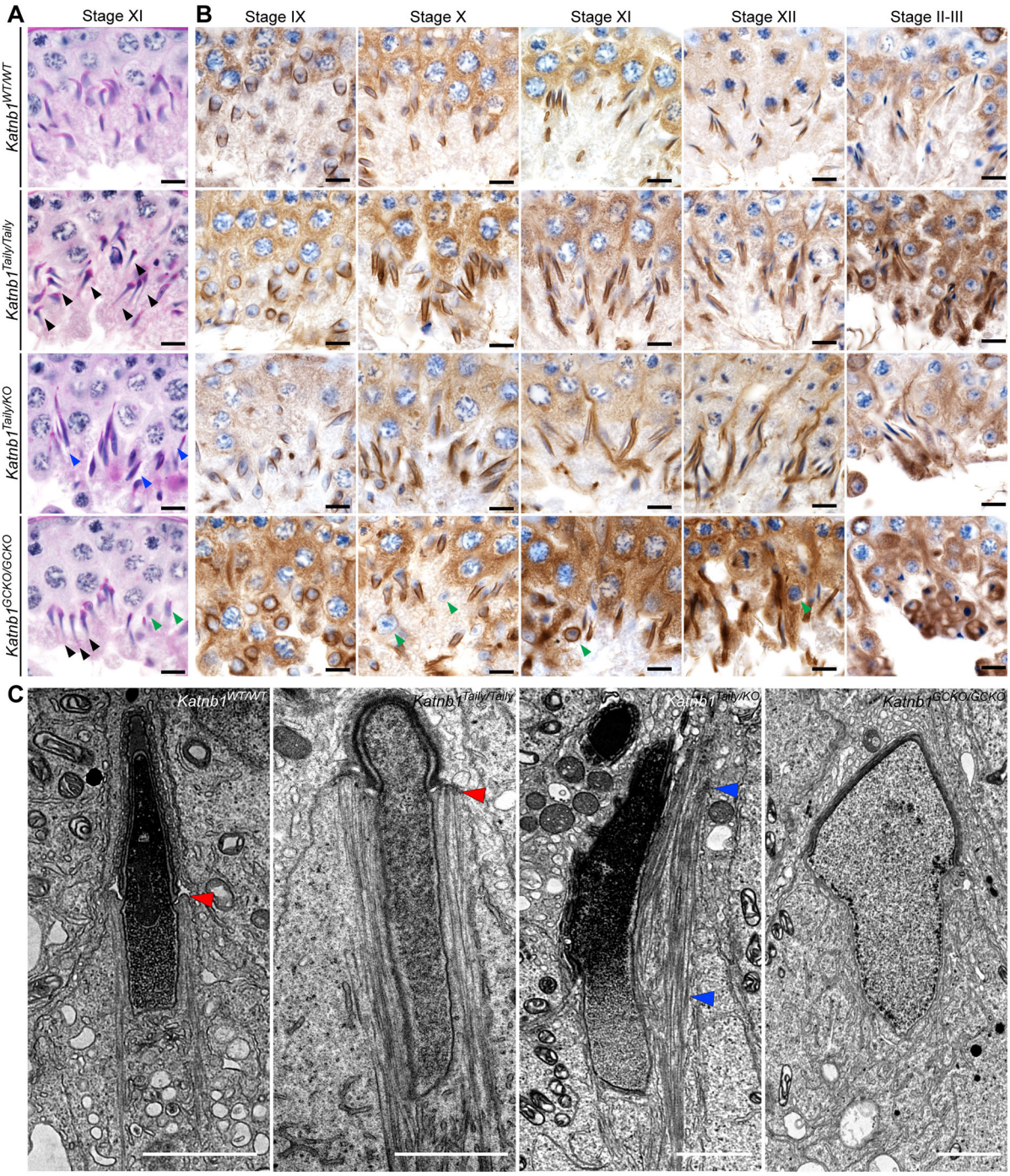

Fig. 7. KATNB1 has both Sertoli- and germ cell-specific roles in sperm head shaping. (A) PAS-stained testis sections showing KATNB1 LOF elongating spermatids. Black arrowheads indicate spermatid nuclei with abnormal 'knobby-head' phenotype. Blue arrowheads indicate spermatid nuclei with abnormal blade-shaped morphology. Green arrowheads indicate spermatid nuclei that failed to elongate. (B) Testis sections immunolabelled for manchettes with α-tubulin antibody in KATNB1 LOF mice. Progressive steps of manchette formation, migration and dissolution are shown left to right. Green arrowheads indicate spermatid nuclei that have failed to elongate. (C) TEM showing nuclear morphology and manchette structure in KATNB1 LOF elongating spermatids. Red arrowheads indicate the perinuclear ring. Blue arrowheads indicate ectopic abnormal manchette-like MTs in *Katnb1*$^{Taily/KO}$ elongating spermatids. Scale bars: 10 µm (A,B); 2 µm (C).

manchette and that perturbations in this process lead to misshapen and detached manchettes.

The seminiferous epithelium and Sertoli cell cytoskeleton are disrupted in all three KATNB1 LOF models

In all three mutant models, KATNB1 loss resulted in pronounced defects in seminiferous epithelium architecture. Germ cells were frequently incorrectly orientated relative to the basement membrane and/or positioned abnormally within the seminiferous epithelium depth (Fig. 2D). As mentioned above, in *Katnb1*$^{Taily/KO}$ and *Katnb1*$^{GCKO/GCKO}$ mutants in particular, germ and Sertoli cell symplasts were frequent and, most obviously, there was frequent loss of Sertoli-germ cell adhesion (Fig. 2D). Accordingly, large sections of epithelium were devoid of germ cells, and Sertoli cells

Development (2021) 148, dev199922. doi:10.1242/dev.199922

had large spaces between cytoplasmic extensions, suggestive of germ cell loss.

This phenotype is reminiscent of *Katnal1*$^{1H/1H}$ mice, in which a *Katnal1* point mutation resulted in seminiferous epithelium disorganisation and premature germ cell sloughing (Smith et al., 2012). In the Smith study, Sertoli cell MTs were disorganised, and it was concluded that compromised epithelial and Sertoli-germ cell junction integrity contributed to the precocious germ cell sloughing of the *Katnal1*$^{1H/1H}$ testis. Sertoli cell MTs (marked by the Sertoli cell-specific β-tubulin isoform TUBB3) were similarly abnormal in *Katnb1* mutant mice (Fig. S7A). MTs were enriched in areas of Sertoli cell cytoplasm devoid of germ cells, and around pyknotic cells (Fig. S7A, black arrowheads). Given that the Sertoli MT cytoskeleton was abnormal in the *Katnb1*$^{GCKO/GCKO}$ mice, which should retain Sertoli cell KATNB1, this phenotype is likely secondary to germ cell loss.

The observed phenotypes are also consistent with abnormalities in ectoplasmic specialisations (ESs), which maintain Sertoli-germ (apical ES) and Sertoli-Sertoli cell adhesion (basal ES) (Dunleavy et al., 2019a). Basal ES junctions (marked by espin) were present in *Katnb1* mutant mice (Fig. S7B,C) and their ultrastructure appeared overtly normal (Fig. S7D). Likewise, in *Katnb1* mutant mice apical ES formation initiated normally between step 8 spermatids and Sertoli cells (Fig. S7C, Stage VIII) and TEM confirmed their presence (Figs 5E,H,K,N,Q,P, 7C, Fig. S6B). However, as spermiogenesis progressed ectopic ES tracts accumulated in disorganised areas of the seminiferous epithelium and at sites of germ cell loss (Fig. 7B,C).

DISCUSSION

Previously, we showed that complete KATNB1 loss is incompatible with life (Furtado et al., 2017). Similarly, herein we show complete ablation of germ cell *Katnb1* is close to incompatible with long-term germ cell survival, leading to extremely reduced numbers of highly abnormal (teratozoospermic) sperm. KATNB1 is required for numerous aspects of male meiosis, including metaphase spindle organisation, chromosome alignment at the metaphase plate, chromosome segregation during anaphase, and cytokinesis. During haploid germ cell development (spermiogenesis), KATNB1 is essential for acrosome biogenesis, sperm tail formation, nuclear sculpting via both the manchette and Sertoli cell, and finally the release of sperm from the testis via spermiation. Notably, we reveal that KATNB1 is a key determinant of katanin A-subunit stability in the mammalian testis. This is consistent with work in *Drosophila* showing that the katanin B-subunit enhances katanin-dependent MT severing in part by decreasing A-subunit proteasome-dependent degradation (Grode and Rogers, 2015) and suggests that the phenotypes identified herein are due to loss of katanin A-subunit effector function.

Our data establish key roles for KATNB1 in multiple phases of male meiosis and, furthermore, reveal that as meiosis progresses it becomes increasingly reliant on KATNB1. Chromosome segregation and cytokinesis were the most KATNB1-sensitive aspects of meiosis. In contrast, preceding KATNB1-dependent functions in specifying metaphase spindle architecture and dynamics were only apparent when KATNB1 was almost completely ablated. Consistent with its absence from spindle poles, KATNB1 did not play a crucial role in generating the spermatocyte spindle MT bulk, as reflected by the presence of meiotic spindles in the KATNB1 LOF models and compatible with our hypothesis that KATNB1 restrains spermatocyte spindle MT bulk (O'Donnell et al., 2012). Why there is greater reliance on KATNB1 in the latter half of male meiosis requires investigation; however, it is plausibly due to the more dramatic and destructive MT remodelling events required in anaphase and telophase compared with metaphase.

The bulk of meiotic defects observed in our *Katnb1* allelic series are consistent with KATNB1 having roles in regulating spermatocyte spindle dynamics. They suggest a role for mammalian KATNB1 in the poleward movement of kinetochore MTs in metaphase 'flux' (reviewed by Rogers et al., 2005) and anaphase 'Pacman-flux' similar to that seen in *Drosophila* and HEK293 mitotic cells (Jiang et al., 2017; Zhang et al., 2007). Data in HEK293 cells showed that KATNB1 contributes to metaphase spindle flux, with reduced poleward flux in mitotic spindles after *Katnb1* ablation (Jiang et al., 2017). Likewise, in *Drosophila* mitosis, katanin-mediated severing has been shown to be involved in anaphase 'Pacman-flux', whereby it appears to uncap kinetochore MT plus-ends, exposing them to depolymerisation by kinesin-13, and thus driving chromosome segregation (Zhang et al., 2007). Our data showing the misalignment of metaphase chromosomes, uneven chromosome segregation and spermatocytes stalling in metaphase and anaphase as a result of KATNB1 LOF are consistent with KATNB1 executing similar functions during male meiosis.

The consistent localisation of KATNB1-based MT-severing complexes to astral spindle fibres, together with the frequent spindle pole alignment defects in *Katnb1*$^{Taily/KO}$ and *Katnb1*$^{GCKO/GCKO}$ spermatocytes, supports an interlinked role for KATNB1 in astral spindle MT generation and/or regulation and spindle pole alignment. This is consistent with the mitotic functions of KATNB1 in HEK293 cells (Jiang et al., 2017). Notably, the most severe spindle alignment defects in our *Katnb1* allelic series, whereby the two spindle poles were on the same side of the cell, are reminiscent of *Katnb1* KO cultured mouse embryonic fibroblasts (Jin et al., 2017), in which bipolar mitotic spindles form but then collapse into a monoastral spindle. Such a phenotype would explain the varying severity of spindle pole misalignment defects in *Katnb1*$^{Taily/KO}$ and *Katnb1*$^{GCKO/GCKO}$ spermatocytes and is consistent with astral MT dysregulation.

Our data clearly show that KATNB1 is required for cytokinesis at the end of meiosis I, and potentially meiosis II, and are consistent with data from *Trypanosoma brucei* showing that the KATNB1 orthologue KAT80 is required for cytokinesis (Casanova et al., 2009). Spermatogenesis is somewhat unique in that cytokinesis is incomplete and sister germ cells remain connected via intercellular bridges (Greenbaum et al., 2011). Similar to somatic midbody abscission, germ cell midbody to intercellular bridge conversion requires MT removal (Dym and Fawcett, 1971; Weber and Russell, 1987; Greenbaum et al., 2007). Our data thus indicate that KATNB1, and katanin MT severing, are required to remove MTs during this process.

Data from *Katnb1*$^{Taily/KO}$ and *Katnb1*$^{GCKO/GCKO}$ spermatids reveal a previously unknown role for MT severing in acrosome formation, specifically in pro-acrosomal vesicle trafficking and fusion onto the nucleus. During the Golgi phase, our data indicate dysregulation of the cytoskeletal 'railroads' between the Golgi apparatus and the acroplaxome (reviewed by Pleuger et al., 2020). Although in rare cases KATNB1 loss resulted in a failure and/or delay in pro-acrosomal vesicle transport, more commonly it resulted in cargoes adhering to multiple sites on the nuclear surface instead of at a single unifying point. That defects were most severe during the cap phase, suggests that KATNB1-mediated cytoskeleton regulation is more important for pro-acrosomal vesicle transport from the endocytic pathway (contributes from the cap phase

Development (2021) 148, dev199922. doi:10.1242/dev.199922

onwards; Berruti and Paiardi, 2015; Berruti et al., 2010; Gioria et al., 2017) than in transport from the Golgi. Accordingly, the endocytic pathway appears to be more reliant on MT-based transport (Pleuger et al., 2020). The fragmented *Katnb1*$^{Taily/KO}$ and *Katnb1*$^{GCKO/GCKO}$ acrosome morphology could also be consistent with membrane remodelling defects during acrosome vesicle fusion. Although such a role for katanin proteins has not been demonstrated, data increasingly suggest that the closely related MT-severing enzyme spastin has interlinked roles in membrane remodelling and MT regulation (Allison et al., 2013; Lumb et al., 2012; Vietri et al., 2015).

The ectopic vesicles in KATNB1-deficient flagella reveal a new role for katanin proteins in sperm tail development. Previous work by us and others revealed roles for katanin proteins, in mouse spermatids, in basal body docking, axoneme extension and specification of the axoneme central pair and, in mouse ependymal cilia, in retrograde intraflagellar transport (IFT) and cilia resolution (O'Donnell et al., 2012; Dunleavy et al., 2017; Banks et al., 2018). The origin of ectopic vesicles in the absence of KATNB1 requires investigation; however, the most-simple explanation is accumulation due to an IFT defect. Although not ubiquitous in IFT mutant models, ectopic vesicles were seen in *Ift25* (*Hspb11*) and *Ift27* KO mouse sperm flagella (Zhang et al., 2017; Liu et al., 2017) and in *IFT88* and *IFT40* RNAi mutant *Trypanosoma brucei* cilia (Absalon et al., 2008). In addition, the abnormal loading/arrangement of mitochondria into KATNB1-deficient sperm tails raises the possibility that KATNB1 contributes to cytoskeletal-based mechanisms of mitochondrial transport, which are independent of the classical IFT pathway (reviewed by Pleuger et al., 2020).

Sperm-head shaping is especially sensitive to KATNB1 disruption. Even partial KATNB1 reductions disrupted manchette dynamics in a manner consistent with MT-severing loss (failure of distal manchette migration, excessive elongation of manchette MTs, delayed manchette dissolution) and consistent with *Katnal2* mutant mouse phenotypes (Dunleavy et al., 2017). Complete ablation of germ cell KATNB1 revealed additional roles in manchette formation, indicating that KATNB1-regulated MT severing plays roles in both generation and remodelling of manchette MTs.

The unique *Katnb1*$^{Taily/KO}$ sperm head phenotype suggests for the first time that KATNB1 is integral for Sertoli cell cytoskeletal dynamics. Whereas the manchette sculpts the spermatid distal nuclear half, the apical half is thought to be shaped by the surrounding Sertoli cell, in conjunction with the acrosome-acroplaxome complex. The lack of the characteristic apical nuclear hook in *Katnb1*$^{Taily/KO}$ spermatids is thus consistent with KATNB1 playing a role in the organisation of, and/or forces generated by, the Sertoli cell cytoskeleton. Moreover, the unique manchette defects of the *Katnb1*$^{Taily/KO}$ mice, indicate that Sertoli cell abnormalities compromise manchette formation and/or ongoing integrity.

Regarding the katanin A-subunits executing KATNB1 testis functions, our data suggest an important role for KATNB1-KATNAL1 complexes in meiosis and Sertoli-germ cell adhesion and, by extension, in maintaining the integrity of the seminiferous epithelium. This latter phenotype is reflected in a previously published model of *Katnal1* hypomorphic function (Smith et al., 2012). Although the previous *Katnal1* hypomorph data suggested that KATNAL1 function was essential in Sertoli cells, a close inspection of the images within this paper reveals the presence of meiotic spindle defects (Smith et al., 2012). A meiotic role is also supported by the notable expression of *Katnal1* in germ cells (Jung et al., 2019) and thus requires future confirmation. Consistent with our previously published work on KATNAL2 (Dunleavy et al., 2017), we predict that KATNB1-KATNAL2 complexes play dominant roles in haploid germ cell development, specifically in manchette dynamics, and by extension nuclear remodelling, and in sperm release. Comparing this study with the *Katnal2* mutant study also confirms that KATNAL2 has autonomous, i.e. KATNB1-independent, functions in spermatogenesis. During tail development, KATNAL2, but not KATNB1, is required for basal body-cell membrane docking and for axoneme extension (Dunleavy et al., 2017). Although KATNB1 contributes to sperm tail development, in its absence sperm tails do form, albeit abnormally. The role of the eponymous A-subunit, KATNA1, within male germ cell development remains untested. Based on the expression presented here, however, we predict that it will have lesser roles than that seen in female meiosis in unicellular organisms. The katanin A-subunit(s) involved in executing KATNB1 functions in other key spermatogenic processes, including acrosome biogenesis and sperm tail development, remain unclear.

This study establishes KATNB1 as a master MT-severing regulator during spermatogenesis, required for regulation of almost all key MT-based structures. Our data suggest that KATNB1 can differentially regulate such a diverse range of structures within this one developmental process by complexing with a 'toolbox' of different katanin A-subunit types. Together with the phenotypes reported in katanin A-subunit mutant mice (Dunleavy et al., 2017; Smith et al., 2012), our findings suggest that during evolution the katanin family has undergone a process of gene duplication and neofunctionalisation to ensure the 'custom cutting' of specific structures during spermatogenesis.

MATERIALS AND METHODS

Mouse model production and phenotypic analysis

All animal procedures were approved by the Monash University School of Biological Sciences Animal Experimentation Ethics Committee and the University of Melbourne Ethics Committee and conducted in accordance with National Health and Medical Research Council (NHMRC) Guidelines on Ethics in Animal Experimentation. The Taily mouse line (*Katnb1*$^{Taily/Taily}$), which contains a point mutation in the N-terminal WD40 domain of *Katnb1* (Fig. 1A,B, red arrowhead), was produced and validated as previously described on a CBA background (O'Donnell et al., 2012), and for the purposes of the current study was backcrossed onto a C57BL/6 background for ten generations. *Katnb1* KO-first conditional-ready mice (*Katnb1*$^{KO/KO}$) were generated through the Monash University Node of the Australian Phenomics Network using a EUCOMM KO-first conditional-ready embryonic stem cell clone (Fig. 1C, HEPD0636_3_G09) as previously described (Cotton et al., 2015; Furtado et al., 2017). To generate mice heterozygous for both the *Taily* allele and the *Katnb1* KO allele (*Katnb1*$^{Taily/KO}$), *Katnb1*$^{KO/WT}$ and *Katnb1*$^{Taily/WT}$ mice were interbred. To generate *Katnb1* germ cell-specific KO mice (*Katnb1*$^{GCKO/GCKO}$), a three-step breeding strategy was used: (1) The conditional *Katnb1* allele (*Katnb1*$^{Flox/Flox}$) was generated by crossing *Katnb1*$^{KO/KO}$ mice with a transgenic line expressing the *Flp* recombinase gene. This resulted in removal of the *FRT* flanked gene-trap cassette, exposing a floxed *Katnb1* exon 4 and reverting mice to a wild-type phenotype. (2) *Katnb1*$^{Flox/Flox}$ females were then mated with *Stra8-Cre* males (Sadate–Ngatchou et al., 2008) to produce *Katnb1*$^{WT/Flox\ Stra8\text{-}Cre}$ males. (3) Finally, *Katnb1*$^{WT/Flox\ Stra8\text{-}Cre}$ males were mated with *Katnb1*$^{Flox/Flox}$ females to produce *Katnb1*$^{Flox/Flox\ Stra8\text{-}Cre}$ (*Katnb1*$^{GCKO/GCKO}$) progeny. In these mice, gene disruption relied on Cre-lox recombination-mediated excision of exon 4 (ENSMUSE00000212976), and the *Stra8-Cre* used is expressed from late spermatogonia onwards (Sadate-Ngatchou et al., 2008). All mice were maintained on a C57BL/6 background, with the exception of the *Stra8-Cre* line, which was maintained on an FVB background. To control for background strain effects on phenotype, wild-type siblings were used as controls for *Katnb1*$^{Taily/Taily}$ and *Katnb1*$^{Taily/KO}$ mice. *Katnb1*$^{Flox/Flox}$ mice

Development (2021) 148, dev199922. doi:10.1242/dev.199922

were used as controls for *Katnb1*$^{GCKO/GCKO}$ mice. All male mice used for analysis were adult (>60 days of age) unless otherwise stated. For each strain, mouse genotypes were determined from tail biopsies using real-time PCR with specific probes designed for each allele (Transnetyx). Efficiency of exon excision in *Katnb1*$^{GCKO/GCKO}$ mice and of mRNA stability in *Katnb1*$^{Taily/Taily}$ and *Katnb1*$^{Taily/KO}$ mice was determined by qPCR of isolated germ cells as described below. Protein levels were determined by western blotting of germ cell and testis lysates as described below.

Germ cell isolation

Germ cells were purified using the STAPUT method as detailed by Dunleavy et al. (2019b). For immunofluorescence labelling, cells were fixed in 4% paraformaldehyde for 20 min.

Quantitative qPCR

Total RNA was extracted from purified germ cells using Trizol (Life Technologies), and reverse-transcribed into cDNA using SuperScript III Reverse Transcriptase (Life Technologies). To assess excision of *Katnb1* exon 4 in the *Katnb1*$^{GCKO/GCKO}$ mice and *Katnb1* mRNA stability in *Katnb1*$^{Taily/Taily}$ and *Katnb1*$^{Taily/KO}$ mice, a primer set was designed spanning part of exons 3 and 4 of the *Katnb1* gene (forward 5′-ACC-TGTGGTCCATAAACAAGCCTAA-3′ and reverse 5′-GACTGGGAAC-CAGCTACGATGA-3′). All *Katnb1* qPCRs were performed using SYBR Select Master Mix (Applied Biosystems). Each reaction was performed in duplicate in an Applied Biosystems QuantStudio 3 Real-Time PCR System with the parameters of 50°C for 2 min, 95°C for 10 min followed by 40 cycles of 95°C for 15 s and 60°C for 1 min. *Ppia* was amplified at the same time as an internal control (using 5′-CGTCTCCTTCGAGCTGTTT-3′ forward and 5′-CCCTGGCACATGAATCCT-3′ reverse primers), and all results were normalised to *Ppia* expression. Differential expression was analysed using the $2^{-\Delta\Delta CT}$ method (Livak and Schmittgen, 2001).

Infertility characterisation

Male infertility phenotypes of the three *Katnb1* mutant mouse lines were defined as outlined by Houston et al. (2020). Testis DSP and total epididymal sperm content were determined using a version of the Triton X-100 solubilisation method described by Cotton et al. (2006) (n≥3/genotype) with minor modifications to increase the reproducibility of counting. Briefly, all cells and nuclei other than condensed elongated spermatid were lysed by homogenisation of whole testes or epididymides in DSP buffer (0.9% NaCl, 0.01% NaN_3, 0.05% Triton X-100; 1 ml per testis or epididymis). To remove residual sperm tails and any remaining uncondensed cells, samples were then sonicated using a 125W probe sonicator (Q125 Sonicator, Qsonica) set at 30% amplitude for 3×10 s cycles with 10 s intervals between cycles. The number of elongated spermatids/sperm per testis and epididymis was then determined using a haemocytometer. Testis DSP rates were calculated by multiplying the number of sperm per testis by 4.84 (time divisor, i.e. the number of days elongated spermatids reside in the mouse testis; Russell et al., 1990).

For histology, testis and epididymal tissue were fixed in Bouin's fixative and histology was assessed using standard methods. PAS and Haematoxylin staining were used to stain male reproductive tract histology and Haematoxylin and Eosin staining was used to visualise air-dried caudal epididymal sperm smears (n≥3/genotype). Germ cell apoptosis was evaluated by immunostaining for cleaved caspase 3 and 9 as described previously (O'Bryan et al., 2013). The number of caspase-positive cells in a minimum of 90 randomly selected seminiferous tubules per mouse were counted and statistical analysis conducted as detailed below (n≥3 mice/genotype). Acrosome abnormalities were quantified by scoring all spermatids in a minimum of three stage XI seminiferous tubule cross-sections per mouse as having either normal or abnormal acrosome morphology. Statistical analysis was conducted as detailed below (n≥3 mice /genotype).

TEM

For analysis of seminiferous tubule ultrastructure, partially decapsulated testes were fixed with 5% glutaraldehyde/4% paraformaldehyde/0.02% picric acid in 0.1 M sodium cacodylate buffer, pH 7.4. Sperm were backflushed as per Baker et al. (2014) from cauda epididymides directly into a fixative solution of 1.7% glutaraldehyde/2% paraformaldehyde/0.02% picric acid /3.2 mM $CaCl_2$/2 mM $MgSO_4$ in 0.1 M sodium cacodylate buffer, pH 7.4. Both testes and sperm were fixed overnight at 4°C and osmicated with 2% osmium tetroxide in 0.1 M sodium cacodylate buffer. Testes samples were *en bloc* stained with 2% uranyl acetate and all samples were embedded into Epon resin using standard procedures. Ultrathin sections were cut on a Reichert Jung Ultracut Microtome and placed on Copper 100×100 square grids (ProSciTech). Sections were analysed using a Jeol JEM-1400 Plus Transmission Electron Microscope in the Monash Ramaciotti Centre for Cryo-Electron Microscopy (Monash University, Clayton, Australia).

Antibody production and use

Synthetic peptides were produced by Mimotopes (Clayton, Australia). Peptides were conjugated to maleimide-activated mcKLH, and the conjugate dialysed against PBS and a final purification buffer of 0.083 M sodium phosphate/0.9 M sodium chloride/0.1 M sorbitol. A KATNB1 polyclonal antibody was produced by immunising goats with a peptide (CSKPQRVKHNSESERRRSPSS) encoding amino acids 74-96 of mouse KATNB1 (Antibodies Australia, Werribee, Australia). A rat monoclonal KATNA1 antibody was produced by the Monash Monoclonal Antibody Facility as described previously (Lo et al., 2012) using a peptide (LDITSLQAAQHELPAAEGEC) encoding amino acids 80-98 of mouse KATNA1. A KATNAL1-specific polyclonal antibody was produced by immunising rabbits with a mix of two peptides (RDPATKAKWQQVRQC and ESFKMDKPPDFPVSC) encoding amino acids 44-57 and 74-88, respectively, of mouse KATNAL1 (Walter and Eliza Hall Institute Antibody Facility, Bundoora, Australia). For the KATNB1 and KATNAL1 antibodies, specific immunoglobulins were purified using the immunising peptide as described previously (Dunleavy et al., 2017). To test their specificity, pre-absorption of each antibody with a molar excess of their corresponding immunising peptides was conducted, followed by immunodetection assays (Fig. S8).

Other primary antibodies used included those against acetylated-tubulin (T6793, Sigma-Aldrich, RRID: Ab_477585, ascites fluid, 1:10,000), actin (A2066, Sigma-Aldrich, 0.67 µg ml^{-1}), α-tubulin (T5168, Sigma-Aldrich, ascites fluid, 1:5000 for immunofluorescence, 1:50,000 for immunohistochemistry; ab4074, Abcam, 1 µg ml^{-1}), cleaved-caspase 3 (9664, Cell Signaling Technology, 0.5 µg ml^{-1}), cleaved-caspase 9 (9509, Cell Signaling Technology, 1 µg ml^{-1}), CLIP170 (sc-28325, Santa Cruz Biotechnology, 0.5 µg ml^{-1}), espin (611656, BD Transduction Laboratories, 0.63 µg ml^{-1}), γ-tubulin (ab11317, Abcam, 5 µg ml^{-1}), KATNAL2 (as described previously; Dunleavy et al., 2017)), KATNB1 (HPA041165, Sigma-Aldrich, 2.4 µg ml^{-1}) and TUBB3 (SAB3300047, Sigma-Aldrich, 0.15 µg ml^{-1}). Secondary antibodies included Alexa Fluor 488 donkey anti-mouse (A212062, Invitrogen), Alexa Fluor 488 donkey anti-rabbit (A21206, Invitrogen), Alexa Fluor 555 donkey anti-goat (A11055, Invitrogen), Alex Fluor 555 donkey anti-mouse (A31570, Invitrogen), Alex Fluor 555 donkey anti-rabbit (A31572, Invitrogen), Alexa Fluor 647 donkey anti-rabbit (A31573, Invitrogen) and EnVision+ Dual Link System-HRP (K4063, Dako). The specificity of immunolabelling was determined by staining sections in parallel in the absence of primary antibody or, where available, KO mouse tissue.

Western blotting

Proteins were extracted from whole testis homogenates and purified germ cells, and immunoblotting conducted as previously described (Dunleavy et al., 2019b). Images were captured using a ChemiDoc MP Imaging System (Bio-Rad). The molecular weights of detected proteins were estimated using a PageRuler Plus Prestained Protein Ladder (Thermo Fisher) and the Image Lab 6.0 Molecular Weight Analysis Tool (Bio-Rad).

Immunochemistry and imaging

Testis immunochemistry was conducted as previously described (Jamsai et al., 2008). To define protein localisation in isolated germ cells, cells were

Development (2021) 148, dev199922. doi:10.1242/dev.199922

permeabilised in 0.2% Triton X-100 in PBS for 20 min at room temperature. Non-specific binding was minimised by blocking with CAS-Block (Invitrogen) for a minimum of 30 min. Primary antibodies were diluted in Dako antibody diluent and incubated overnight at 4°C. Secondary antibodies were diluted 1 in 500 and incubated at room temperature for 1 h. DNA was visualised using 1 µg ml^{-1} 4′,6-diamidino-2-phenylindole (DAPI, Invitrogen) and acrosomes were visualised using 0.5 µg ml^{-1} lectin peanut agglutinin (PNA), Alexa Fluor 488 conjugate (L21409, Life Technologies).

To determine the subcellular localisation of KATNB1 bound to each of the katanin A-subunits, Duolink *in situ* PLAs were carried out as per the manufacturer's instructions (Olink Bioscience) and as described previously (Dunleavy et al., 2017). The specificity of the assay was determined by staining parallel samples in the absence of either both, or one of, the primary antibodies and by the parallel staining of *Katnb1*$^{GCKO/GCKO}$ spermatocytes. Samples were counterstained for MTs and nuclei as described above. Quantitative differences in testis cell apoptosis between genotypes were detected using caspase immunochemistry. Slides were scanned using an Aperio Scanscope AT Turbo (Leica Microsystems) in the Monash Histology Platform (Monash University, Clayton, Australia).

Immunofluorescence images were collected using a Leica TCS SP8 confocal microscope (Leica Microsystems) in the Monash Micro Imaging facility (Monash University, Clayton, Australia). All immunofluorescence images were taken using the 63×/1.40 HC PL APO CS2 oil immersion objective. *z*-stacks of isolated cells were collected with 0.3 µm intervals and assembled into maximum intensity projections in ImageJ 1.47N. Images were adjusted uniformly across the image and between groups.

Statistics

Statistical analysis of germ cell apoptosis data was conducted in R version 3.5.1. (R Core Development Team, 2015). Generalised linear mixed (GLM) models were used to compare the number of caspase-positive cells per tubule across genotypes, with animal ID included as a random effect to account for repeated measures per individual. For each model, Akaike information criteria (AIC) estimates were used to select the most appropriate error distribution and link function (i.e. Poisson, negative binomial, zero-inflated Poisson, zero-inflated negative binomial) using the glmer function (lme4 package; Bates et al., 2015) and glmmTMB function (glmmTMB package; Brooks et al., 2017). For all models, a zero-inflated negative binomial distribution (fitted with glmmTMB, using the ziformula argument) was selected as the most appropriate error distribution and link function (i.e. had the lowest AIC score).

All other statistical analyses were conducted in GraphPad Prism 8.0. The statistical significance of differences between two groups was determined with an unpaired Student's *t*-test and a one-way ANOVA was used to determine differences between more than two groups. Significance was defined as $P<0.05$.

Acknowledgements

We thank Dr Liza O'Donnell and Dr Duangporn Jamsai for advice on the initial stages of the project; Dr Brendan Houston, Dr Denis Korneev, Ms Amy Luan and Ms Lauren Rogers for technical assistance; and Dr Christopher Johnstone for assistance with the statistical analyses.

Competing interests

The authors declare no competing or financial interests.

Author contributions

Conceptualization: J.E.M.D., H.O., M.K.O.; Methodology: J.E.M.D., A.E.O., H.O., D.J.M., M.K.O.; Formal analysis: J.E.M.D., A.E.O., H.O., D.J.M., M.K.O.; Investigation: J.E.M.D., A.E.O., H.O., D.J.M.; Writing - original draft: J.E.M.D., M.K.O.; Writing - review & editing: J.E.M.D., A.E.O., M.K.O.; Visualization: J.E.M.D., A.E.O.; Supervision: M.K.O.; Project administration: J.E.M.D., M.K.O.; Funding acquisition: M.K.O.

Funding

J.E.M.D is supported by a National Health and Medical Research Council Ideas Grant to M.K.O and J.E.M.D (APP1180929) and this project was supported in part by funding from the National Health and Medical Research Council of Australia (APP1138014) and the Australian Research Council (DP160100647). H.O. was funded by Japan Society for the Promotion of Science Research Fellowship for Young Scientists.

Peer review history

The peer review history is available online at https://journals.biologists.com/dev/article-lookup/doi/10.1242/dev.199922.

References

Absalon, S., Blisnick, T., Bonhivers, M., Kohl, L., Cayet, N., Toutirais, G., Buisson, J., Robinson, D. and Bastin, P. (2008). Flagellum elongation is required for correct structure, orientation and function of the flagellar pocket in Trypanosoma brucei. *J. Cell Sci.* **121**, 3704. doi:10.1242/jcs.035626

Allison, R., Lumb, J. H., Fassier, C., Connell, J. W., Ten Martin, D., Seaman, M. N. J., Hazan, J. and Reid, E. (2013). An ESCRT–spastin interaction promotes fission of recycling tubules from the endosome. *J. Cell Biol.* **202**, 527-543. doi:10.1083/jcb.201211045

Baker, M. A., Hetherington, L., Weinberg, A. and Velkov, T. (2014). Phosphopeptide analysis of rodent epididymal spermatozoa. *JoVE (Journal of Visualized Experiments)* **94**, e51546.

Banks, G., Lassi, G., Hoerder-Suabedissen, A., Tinarelli, F., Simon, M. M., Wilcox, A., Lau, P., Lawson, T. N., Johnson, S., Rutman, A. et al. (2018). A missense mutation in katnal1 underlies behavioural, neurological and ciliary anomalies. *Mol. Psychiatry* **23**, 713-722. doi:10.1038/mp.2017.54

Bates, D., Mächler, M., Bolker, B. and Walker, S. (2015). Fitting linear mixed-effects models using lme4. *J. Stat. Softw.* **67**, 1-48.

Berruti, G. and Paiardi, C. (2015). Usp8/ubpy-regulated sorting and the development of sperm acrosome: the recruitment of met. *Reproduction* **149**, 633-644. doi:10.1530/REP-14-0671

Berruti, G., Ripolone, M. and Ceriani, M. (2010). Usp8, a regulator of endosomal sorting, is involved in mouse acrosome biogenesis through interaction with the spermatid ESCRT-0 complex and microtubules1. *Biol. Reprod.* **82**, 930-939. doi:10.1095/biolreprod.109.081679

Brooks, M. E., Kristensen, K., Van Benthem, K. J., Magnusson, A., Berg, C. W., Nielsen, A., Skaug, H. J., Machler, M. and Bolker, B. M. (2017). glmmTMB balances speed and flexibility among packages for zero-inflated generalized linear mixed modeling. *R J.* **9**, 378-400. doi:10.32614/RJ-2017-066

Casanova, M., Crobu, L., Blaineau, C., Bourgeois, N., Bastien, P. and Pagès, M. (2009). Microtubule-severing proteins are involved in flagellar length control and mitosis in trypanosomatids. *Mol. Microbiol.* **71**, 1353-1370. doi:10.1111/j.1365-2958.2009.06594.x

Cheung, K., Senese, S., Kuang, J., Bui, N., Ongpipattanakul, C., Gholkar, A., Cohn, W., Capri, J., Whitelegge, J. P. and Torres, J. Z. (2016). Proteomic analysis of the mammalian katanin family of microtubule-severing enzymes defines katanin p80 subunit b-like 1 (KATNBL1) as a regulator of mammalian katanin microtubule-severing. *Mol. Cell. Proteomics* **15**, 1658-1669. doi:10.1074/mcp.M115.056465

Cotton, L., Gibbs, G. M., Sanchez-Partida, L. G., Morrison, J. R., De Kretser, D. M. and O'bryan, M. K. (2006). Fgfr-1 signaling is involved in spermiogenesis and sperm capacitation. *J. Cell Sci.* **119**, 75-84. doi:10.1242/jcs.02704

Cotton, L. M., Meilak, M. L., Templeton, T., Gonzales, J. G., Nenci, A., Cooney, M., Truman, D., Rodda, F., Lynas, A. and Viney, E. (2015). Utilising the resources of the international knockout mouse consortium: The Australian experience. *Mamm. Genome* **26**, 142-153. doi:10.1007/s00335-015-9555-1

Dunleavy, J. E., Okuda, H., O'connor, A. E., Merriner, D. J., O'donnell, L., Jamsai, D., Bergmann, M. and O'bryan, M. K. (2017). Katanin-like 2 (katnal2) functions in multiple aspects of haploid male germ cell development in the mouse. *PLOS Genet.* **13**, e1007078. doi:10.1371/journal.pgen.1007078

Dunleavy, J. E., O'bryan, M. K., Stanton, P. G. and O'donnell, L. (2019a). The cytoskeleton in spermatogenesis. *Reproduction* **157**, R53-R72. doi:10.1530/REP-18-0457

Dunleavy, J. E. M., O'connor, A. E. and O'bryan, M. K. (2019b). An optimised STAPUT method for the purification of mouse spermatocyte and spermatid populations. *Mol. Hum. Reprod.* **25**, 675-683. doi:10.1093/molehr/gaz056

Dym, M. and Fawcett, D. W. (1971). Further observations on the numbers of spermatogonia, spermatocytes, and spermatids connected by intercellular bridges in the mammalian testis. *Biol. Reprod.* **4**, 195-215. doi:10.1093/biolreprod/4.2.195

Ernst, C., Eling, N., Martinez-Jimenez, C. P., Marioni, J. C. and Odom, D. T. (2019). Staged developmental mapping and x chromosome transcriptional dynamics during mouse spermatogenesis. *Nat. Commun.* **10**, 1251. doi:10.1038/s41467-019-09182-1

Frickey, T. and Lupas, A. N. (2004). Phylogenetic analysis of AAA proteins. *J. Struct. Biol.* **146**, 2-10. doi:10.1016/j.jsb.2003.11.020

Furtado, M. B., Merriner, D. J., Berger, S., Rhodes, D., Jamsai, D. and O'bryan, M. K. (2017). Mutations in the *katnb1* gene cause left–right asymmetry and heart defects. *Dev. Dyn.* **246**, 1027. doi:10.1002/dvdy.24564

Gioria, M., Pasini, M. E. and Berruti, G. (2017). Dynamic of contribution of UBPy-sorted cargo to acrosome biogenesis: Effects of its derailment in a mouse model of globozoospermia, the infertile Vps54 (L967Q) mutant. *Cell Tissue Res.* **369**, 413-427. doi:10.1007/s00441-017-2592-1

Greenbaum, M. P., Ma, L. and Matzuk, M. M. (2007). Conversion of midbodies into germ cell intercellular bridges. *Dev. Biol.* **305**, 389-396. doi:10.1016/j.ydbio.2007.02.025

Greenbaum, M. P., Iwamori, T., Buchold, G. M. and Matzuk, M. M. (2011). Germ cell intercellular bridges. *Cold Spring Harbor Perspect. Biol.* **3**, a005850. doi:10.1101/cshperspect.a005850

Grode, K. D. and Rogers, S. L. (2015). The non-catalytic domains of drosophila katanin regulate its abundance and microtubule-disassembly activity. *PLoS ONE* **10**, e0123912. doi:10.1371/journal.pone.0123912

Guo, J., Grow, E. J., Mlcochova, H., Maher, G. J., Lindskog, C., Nie, X., Guo, Y., Takei, Y., Yun, J., Cai, L. et al. (2018). The adult human testis transcriptional cell atlas. *Cell Res.* **28**, 1141-1157. doi:10.1038/s41422-018-0099-2

Hartman, J. J., Mahr, J., Mcnally, K., Okawa, K., Iwamatsu, A., Thomas, S., Cheesman, S., Heuser, J., Vale, R. D. and Mcnally, F. J. (1998). Katanin, a microtubule-severing protein, is a novel AAA ATPase that targets to the centrosome using a WD40-containing subunit. *Cell* **93**, 277-287. doi:10.1016/S0092-8674(00)81578-0

Houston, B. J., Conrad, D. F. and O'bryan, M. K. (2020). A framework for high-resolution phenotyping of candidate male infertility mutants: From human to mouse. *Hum. Genet.* **140**, 155-182. doi:10.1007/s00439-020-02159-x

Hu, W. F., Pomp, O., Ben-Omran, T., Kodani, A., Henke, K., Mochida, G. H., Timothy, W. Y., Woodworth, M. B., Bonnard, C. and Raj, G. S. (2014). Katanin p80 regulates human cortical development by limiting centriole and cilia number. *Neuron,* **84**, 1240-1257. doi:10.1016/j.neuron.2014.12.017

Jamsai, D., Bianco, D. M., Smith, S. J., Merriner, D. J., Ly-Huynh, J. D., Herlihy, A., Niranjan, B., Gibbs, G. M. and O'bryan, M. K. (2008). Characterization of gametogenetin 1 (GGN1) and its potential role in male fertility through the interaction with the ion channel regulator, cysteine-rich secretory protein 2 (CRISP2) in the sperm tail. *Reproduction* **135**, 751-760. doi:10.1530/REP-07-0485

Jiang, K., Rezabkova, L., Hua, S., Liu, Q., Capitani, G., Altelaar, A. M., Heck, A. J., Kammerer, R. A., Steinmetz, M. O. and Akhmanova, A. (2017). Microtubule minus-end regulation at spindle poles by an ASPM-katanin complex. *Nat. Cell Biol.* **19**, 480-492. doi:10.1038/ncb3511

Jin, M., Pomp, O., Shinoda, T., Toba, S., Torisawa, T., Furuta, K. Y., Oiwa, K., Yasunaga, T., Kitagawa, D. and Matsumura, S. (2017). Katanin p80, NuMA and cytoplasmic dynein cooperate to control microtubule dynamics. *Sci. Rep.* **7**, 1-16. doi:10.1038/s41598-016-0028-x

Joly, N., Martino, L., Gigant, E., Dumont, J. and Pintard, L. (2016). Microtubule-severing activity of the AAA+ ATPase katanin is essential for female meiotic spindle assembly. *Development* **143**, 3604-3614. doi:10.1242/dev.140830

Jung, M., Wells, D., Rusch, J., Ahmad, S., Marchini, J., Myers, S. R. and Conrad, D. F. (2019). Unified single-cell analysis of testis gene regulation and pathology in five mouse strains. *eLife* **8**, e43966. doi:10.7554/eLife.43966

Liu, H., Li, W., Zhang, Y., Zhang, Z., Shang, X., Zhang, L., Zhang, S., Li, Y., Somoza, A. V., Delpi, B. et al. (2017). Ift25, an intraflagellar transporter protein dispensable for ciliogenesis in somatic cells, is essential for sperm flagella formation. *Biol. Reprod.* **96**, 993-1006. doi:10.1093/biolre/iox029

Livak, K. J. and Schmittgen, T. D. (2001). Analysis of relative gene expression data using real-time quantitative PCR and the $2^{-\Delta\Delta CT}$ method. *Methods* **25**, 402-408. doi:10.1006/meth.2001.1262

Lo, J. C., Jamsai, D., O'connor, A. E., Borg, C., Clark, B. J., Whisstock, J. C., Field, M. C., Adams, V., Ishikawa, T. and Aitken, R. J. (2012). Rab-like 2 has an essential role in male fertility, sperm intra-flagellar transport, and tail assembly. *PLoS Genet.* **8**, e1002969. doi:10.1371/journal.pgen.1002969

Lumb, J. H., Connell, J. W., Allison, R. and Reid, E. (2012). The AAA ATPase spastin links microtubule severing to membrane modelling. *Biochim. Biophys. Acta.* **1823**, 192-197. doi:10.1016/j.bbamcr.2011.08.010

Mcnally, K. P. and Mcnally, F. J. (2011). The spindle assembly function of Caenorhabditis elegans katanin does not require microtubule-severing activity. *Mol. Biol. Cell* **22**, 1550-1560. doi:10.1091/mbc.e10-12-0951

Mcnally, F. J. and Roll-Mecak, A. (2018). Microtubule-severing enzymes: From cellular functions to molecular mechanism. *J. Cell Biol.* **217**, 4057-4069. doi:10.1083/jcb.201612104

Mcnally, K. P., Bazirgan, O. A. and Mcnally, F. J. (2000). Two domains of p80 katanin regulate microtubule severing and spindle pole targeting by p60 katanin. *J. Cell Sci.* **113**, 1623-1633. doi:10.1242/jcs.113.9.1623

McNally, K., Audhya, A., Oegema, K. and Mcnally, F. J. (2006). Katanin controls mitotic and meiotic spindle length. *J. Cell Biol.* **175**, 881-891. doi:10.1083/jcb.200608117

Mishra-Gorur, K., Çağlayan, A. O., Schaffer, A. E., Chabu, C., Henegariu, O., Vonhoff, F., Akgümüş, G. T., Nishimura, S., Han, W. and Tu, S. (2014). Mutations in KATNB1 cause complex cerebral malformations by disrupting asymmetrically dividing neural progenitors. *Neuron* **84**, 1226-1239. doi:10.1016/j.neuron.2014.12.014

O'bryan, M. K., Clark, B. J., Mclaughlin, E. A., D'sylva, R. J., O'donnell, L., Wilce, J. A., Sutherland, J., O'connor, A. E., Whittle, B. and Goodnow, C. C. (2013). Rbm5 is a male germ cell splicing factor and is required for spermatid differentiation and male fertility. *PLoS Genet.* **9**, e1003628. doi:10.1371/journal.pgen.1003628

O'donnell, L., Rhodes, D., Smith, S. J., Merriner, D. J., Clark, B. J., Borg, C., Whittle, B., O'connor, A. E., Smith, L. B. and Mcnally, F. J. (2012). An essential role for katanin p80 and microtubule severing in male gamete production. *PLoS Genet.* **8**, e1002698. doi:10.1371/journal.pgen.1002698

Oko, R. and Sutovsky, P. (2009). Biogenesis of sperm perinuclear theca and its role in sperm functional competence and fertilization. *J. Reprod. Immunol.* **83**, 2-7. doi:10.1016/j.jri.2009.05.008

Pleuger, C., Lehti, M. S., Dunleavy, J. E., Fietz, D. and O'bryan, M. K. (2020). Haploid male germ cells – the grand central station of protein transport. *Hum. Reprod. Update* **26**, 474-500. doi:10.1093/humupd/dmaa004

R Core Development Team (2015). R: A language and environment for statistical computing. R Foundation for Statistical Computing.

Rezabkova, L., Jiang, K., Capitani, G., Prota, A. E., Akhmanova, A., Steinmetz, M. O. and Kammerer, R. A. (2017). Structural basis of katanin p60: P80 complex formation. *Sci. Rep.* **7**, 14893-14893. doi:10.1038/s41598-017-14194-2

Rogers, G. C., Rogers, S. L. and Sharp, D. J. (2005). Spindle microtubules in flux. *J. Cell Sci.* **118**, 1105-1116. doi:10.1242/jcs.02284

Russell, L. D. E., Robert , A., Sinha, H., Amiya, P. and Clegg, E. D. (1990). *Histological and Histopathological Evaluation of the Testis*. Clearwater, Florida: Cache River Press.

Sadate–Ngatchou, P. I., Payne, C. J., Dearth, A. T. and Braun, R. E. (2008). Cre recombinase activity specific to postnatal, premeiotic male germ cells in transgenic mice. *Genesis* **46**, 738-742. doi:10.1002/dvg.20437

Smith, L. B., Milne, L., Nelson, N., Eddie, S., Brown, P., Atanassova, N., O'bryan, M. K., O'donnell, L., Rhodes, D. and Wells, S. (2012). KATNAL1 regulation of Sertoli cell microtubule dynamics is essential for spermiogenesis and male fertility. *PLOS Genet.* **8**, e1002697. doi:10.1371/journal.pgen.1002697

Srayko, M., Buster, D. W., Bazirgan, O. A., Mcnally, F. J. and Mains, P. E. (2000). MEI-1/MEI-2 katanin-like microtubule severing activity is required for Caenorhabditis elegans meiosis. *Genes Dev.* **14**, 1072-1084. doi:10.1101/gad.14.9.1072

Vale, R. D. (1991). Severing of stable microtubules by a mitotically activated protein in Xenopus egg extracts. *Cell,* **64**, 827-839. doi:10.1016/0092-8674(91)90511-V

Vemu, A., Szczesna, E., Zehr, E. A., Spector, J. O., Grigorieff, N., Deaconescu, A. M. and Roll-Mecak, A. (2018). Severing enzymes amplify microtubule arrays through lattice GTP-tubulin incorporation. *Science* **361**, eaau1504. doi:10.1126/science.aau1504

Vietri, M., Schink, K. O., Campsteijn, C., Wegner, C. S., Schultz, S. W., Christ, L., Thoresen, S. B., Brech, A., Raiborg, C. and Stenmark, H. (2015). Spastin and ESCRT-III coordinate mitotic spindle disassembly and nuclear envelope sealing. *Nature,* **522**, 231-235. doi:10.1038/nature14408

Wang, M., Liu, X., Chang, G., Chen, Y., An, G., Yan, L., Gao, S., Xu, Y., Cui, Y., Dong, J. et al. (2018). Single-cell RNA sequencing analysis reveals sequential cell fate transition during human spermatogenesis. *Cell Stem Cell,* **23**, 599-614.e4. doi:10.1016/j.stem.2018.08.007

Weber, J. E. and Russell, L. D. (1987). A study of intercellular bridges during spermatogenesis in the rat. *Am. J. Anat.* **180**, 1-24. doi:10.1002/aja.1001800102

Zehr, E., Szyk, A., Piszczek, G., Szczesna, E., Zuo, X. and Roll-Mecak, A. (2017). Katanin spiral and ring structures shed light on power stroke for microtubule severing. *Nat. Struct. Mol. Biol.* **24**, 717. doi:10.1038/nsmb.3448

Zehr, E. A., Szyk, A., Szczesna, E. and Roll-Mecak, A. (2020). Katanin grips the β-tubulin tail through an electropositive double spiral to sever microtubules. *Dev. Cell* **52**, 118-131.e6. doi:10.1016/j.devcel.2019.10.010

Zhang, D., Rogers, G. C., Buster, D. W. and Sharp, D. J. (2007). Three microtubule severing enzymes contribute to the 'pacman-flux' machinery that moves chromosomes. *J. Cell Biol.* 177, 231-242. doi:10.1083/jcb.200612011

Zhang, Y., Liu, H., Li, W., Zhang, Z., Shang, X., Zhang, D., Li, Y., Zhang, S., Liu, J., Hess, R. A. et al. (2017). Intraflagellar transporter protein (IFT27), an IFT25 binding partner, is essential for male fertility and spermiogenesis in mice. *Dev. Biol.* **432**, 125-139. doi:10.1016/j.ydbio.2017.09.023

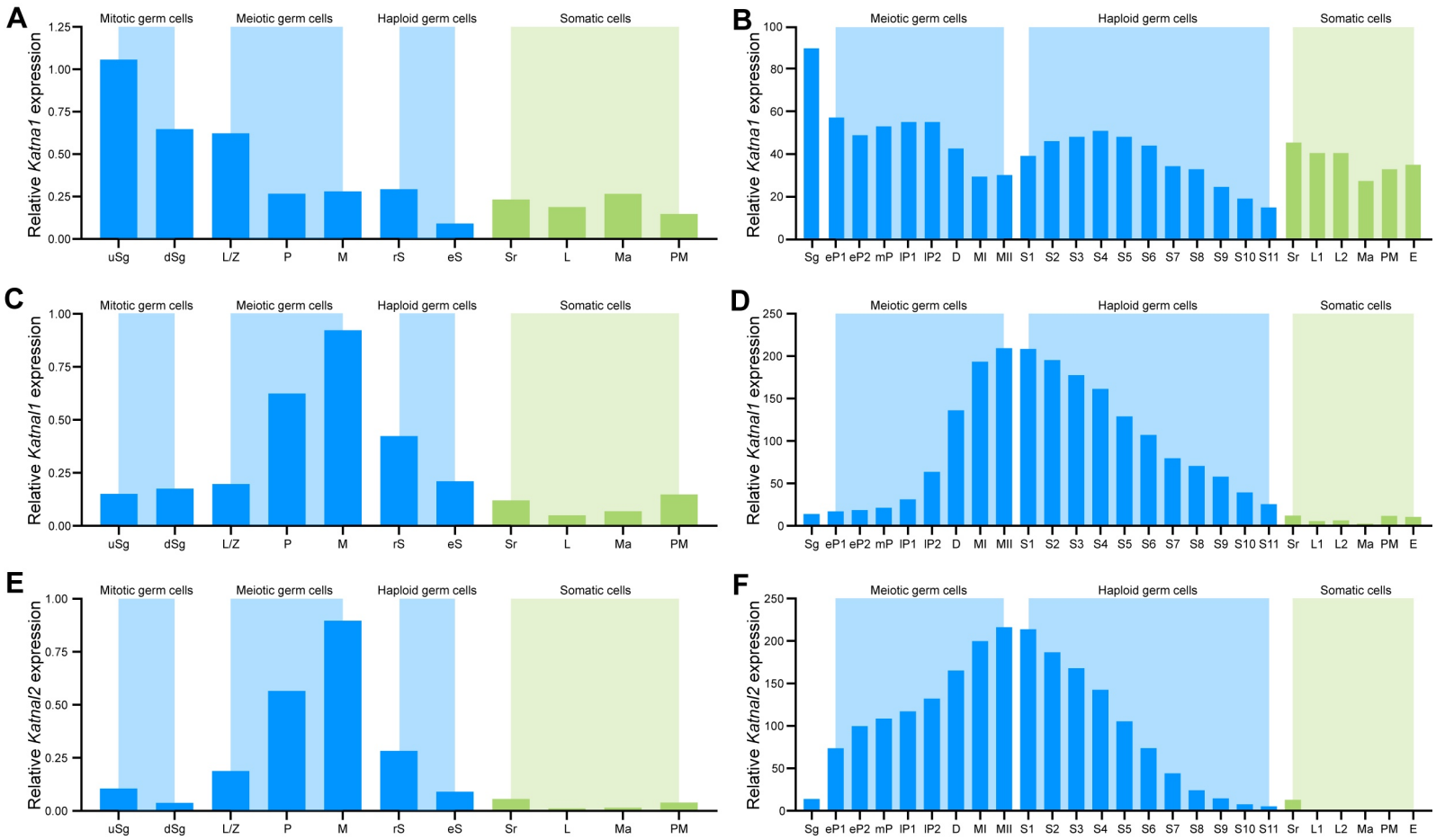

Fig. S1. Katanin A-subunit expression in the adult mouse testis.

Katna1 (**A**, **B**), *Katnal1* (**C**, **D**) and *Katnal2* (**E**, **F**) expression across major cell types in the adult mouse testis as determined by two different single-cell RNA-sequencing studies. **A**,**C**,**E** were extracted from data generated by (Jung et al., 2019) and **B**, **D**, **F** were extracted from data generated by (Ernst et al., 2019). In **A**, **C**, **E**, X-axis left to right: uSg = undifferentiated spermatogonia, dSg = differentiating spermatogonia, L/Z= leptotene/zygotene spermatocytes, P = pachytene spermatocytes, M = meiosis, rS = round spermatids, eS = elongating spermatids, Sr = Sertoli cells, L = Leydig cells, Ma = macrophages, PM = peritubular myoid cells. In **B**, **D**, **F**, X-axis left to right: Sg = spermatogonia, eP1-eP2 = early pachytene 1-2 spermatocytes, D = diplotene spermatocytes, MI = meiosis I, MII = meiosis II, S1-S11 = step 1-11 spermatids, Sr = Sertoli cell, L1-2 = Leydig cells 1-2, Ma = macrophages, PM = peritubular myoid cells, E = endothelial cells.

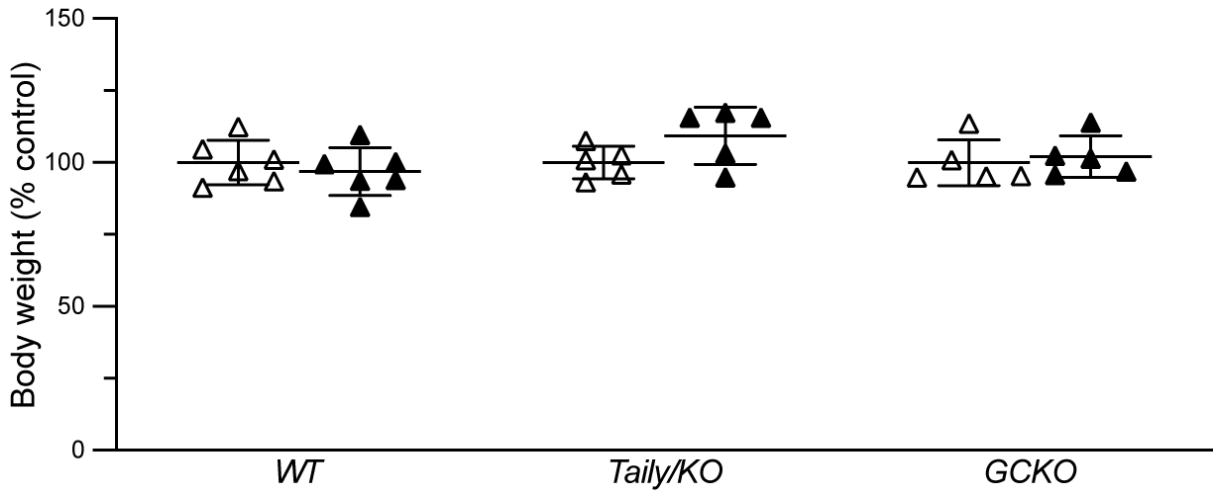

Fig. S2. Body weight of KATNB1 LOF mice.

No difference in overall body weight was observed between strain specific control male mice (white triangles) and either *Katnb1*$^{Taily/Taily}$, *Katnb1*$^{Taily/KO}$ and *Katnb1*$^{GCKO/GCKO}$ (black triangles) male mice. Lines represent mean±s.d., n=4-6 per genotype.

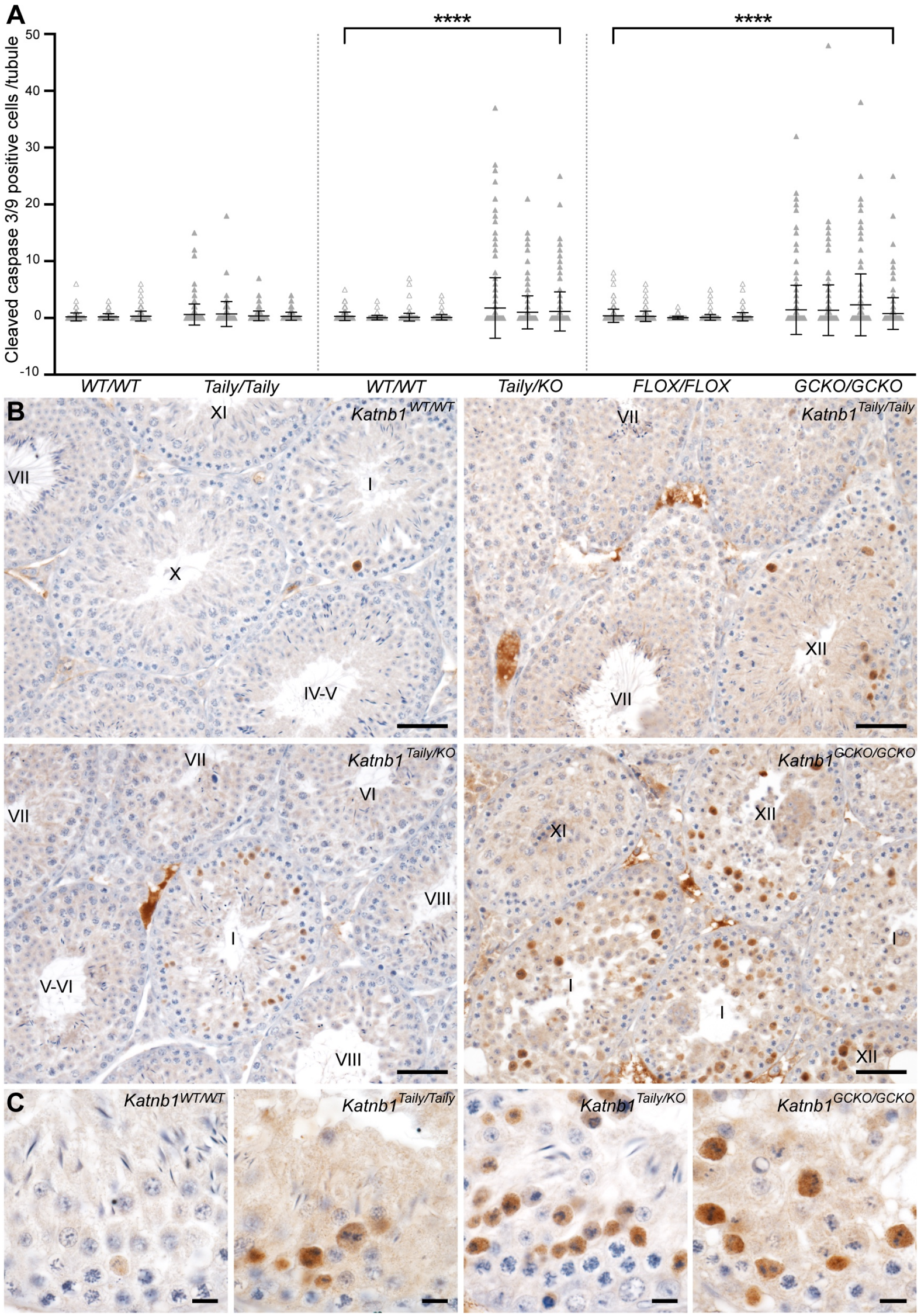

Fig. S3. Loss of KATNB1 results in increased germ cell apoptosis.

Germ cell apoptosis in KATNB1 LOF mice as assessed by immunolabelling of seminiferous tubules for cleaved-caspase 3 and 9. The average number of cleaved-caspase 3 and/or 9 positive germ cells per seminiferous tubule is graphed in (**A**) and representative images of testis immunolabelling of cleaved-caspase 3 and 9 are shown in (**B**-**C**). In (**A**) *Katnb1*$^{Taily/Taily}$, *Katnb1*$^{Taily/KO}$, *Katnb1*$^{GCKO/GCKO}$ mice (white triangles) are graphed compared to their strain specific controls (grey triangles). Sub-columns within each genotype represent individual mice, and lines represent mean±s.d. for each. A minimum of 90 randomly selected seminiferous tubules per mouse were counted (n≥3 mice /genotype). Statistically significant increases in germ cell apoptosis were observed in both *Katnb1*$^{Taily/KO}$ and *Katnb1*$^{GCKO/GCKO}$ compared to their respective controls, **** P<0.0001. Cleaved-caspase 3/9 positive cells were frequently observed in stage XII and I tubules of all KATNB1 LOF genotypes, but rarely seen in other seminiferous tubule stages or in controls (**B**). Higher magnification revealed cleaved-caspase 3/9 positive cells in *Katnb1*$^{Taily/Taily}$, *Katnb1*$^{Taily/KO}$, *Katnb1*$^{GCKO/GCKO}$ stage XII and I tubules were spermatocytes undergoing meiosis (**C**). Scale bars in **B** = 50 μm and in **A** = 10 μm. Roman numerals indicate seminiferous tubule stages in **B.**

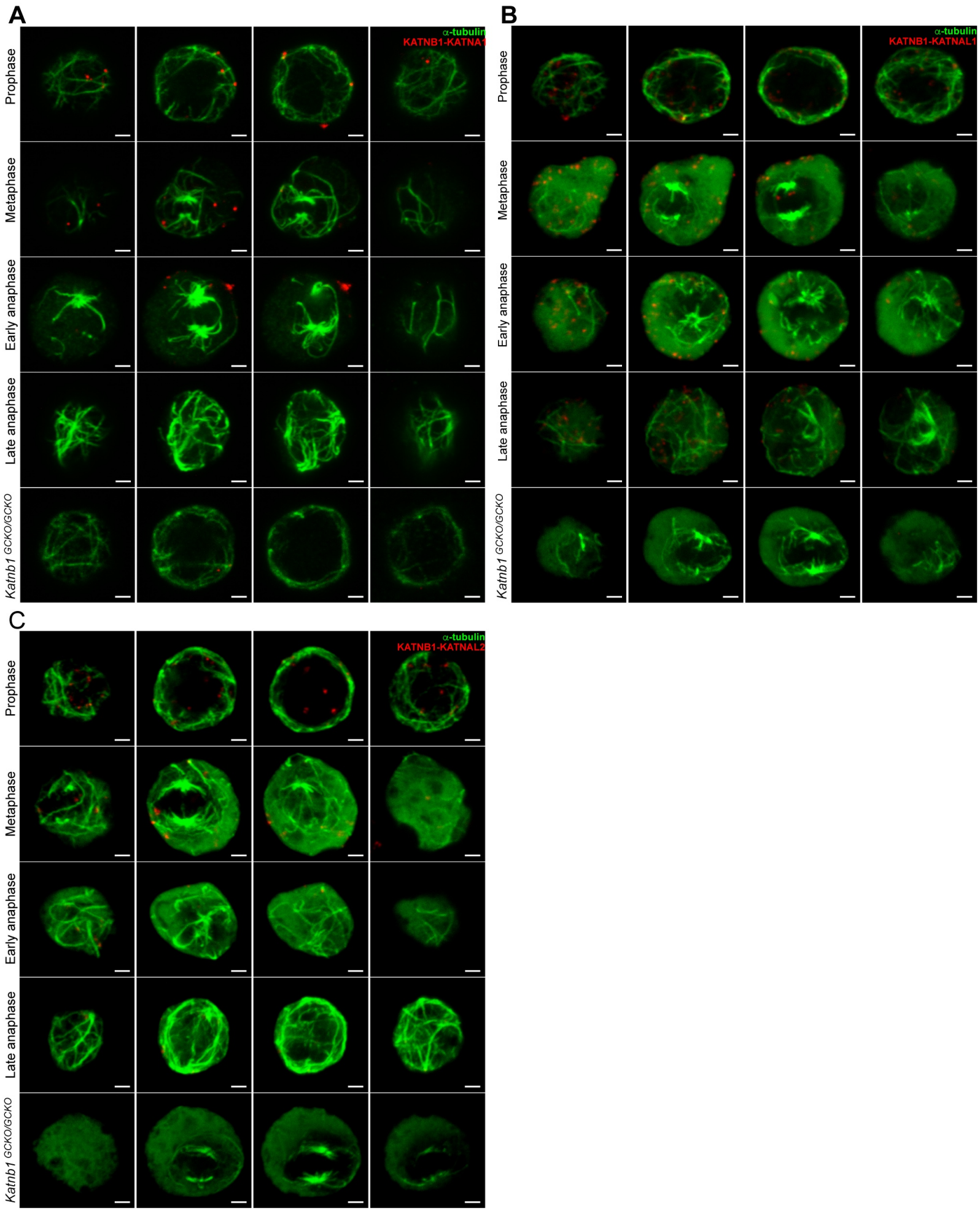

Fig. S4. Precise localisation of KATNB1-based MT severing complexes during mouse male meiosis.

Subgroups of images taken from each Z-stack presented in Fig. 4A-C to allow a more precise localisation of KATNA1-KATNB1 (**A**), KATNAL1-KATNB1 (**B**) and KATNAL2-KATNB1 (**C**) complexes during meiosis. Images represent *in situ* proximity ligation assays using antibodies directed against (**A**) KATNA1 and KATNB1, (**B**) KATNAL1 and KATNB1, and (**C**) KATNAL2 and KATNB1 in isolated *Katnb1*$^{Flox/Flox}$ spermatocytes. Assay specificity was shown by the parallel staining of *Katnb1*$^{GCKO/GCKO}$ spermatocytes. For each assay, spermatocytes from n=3 *Katnb1*$^{Flox/Flox}$ mice and from n=1 *Katnb1*$^{GCKO/GCKO}$ mouse were assessed. Red represents KATNB1-based complexes and green represents MTs as marked by α-tubulin. For each meiotic stage presented, the four images represent different depths within the same cell. Each individual image represents Z-stacks spanning 2.7 μm in the Z-plane presented as 2D maximum intensity projections. Scale bars = 2 μm.

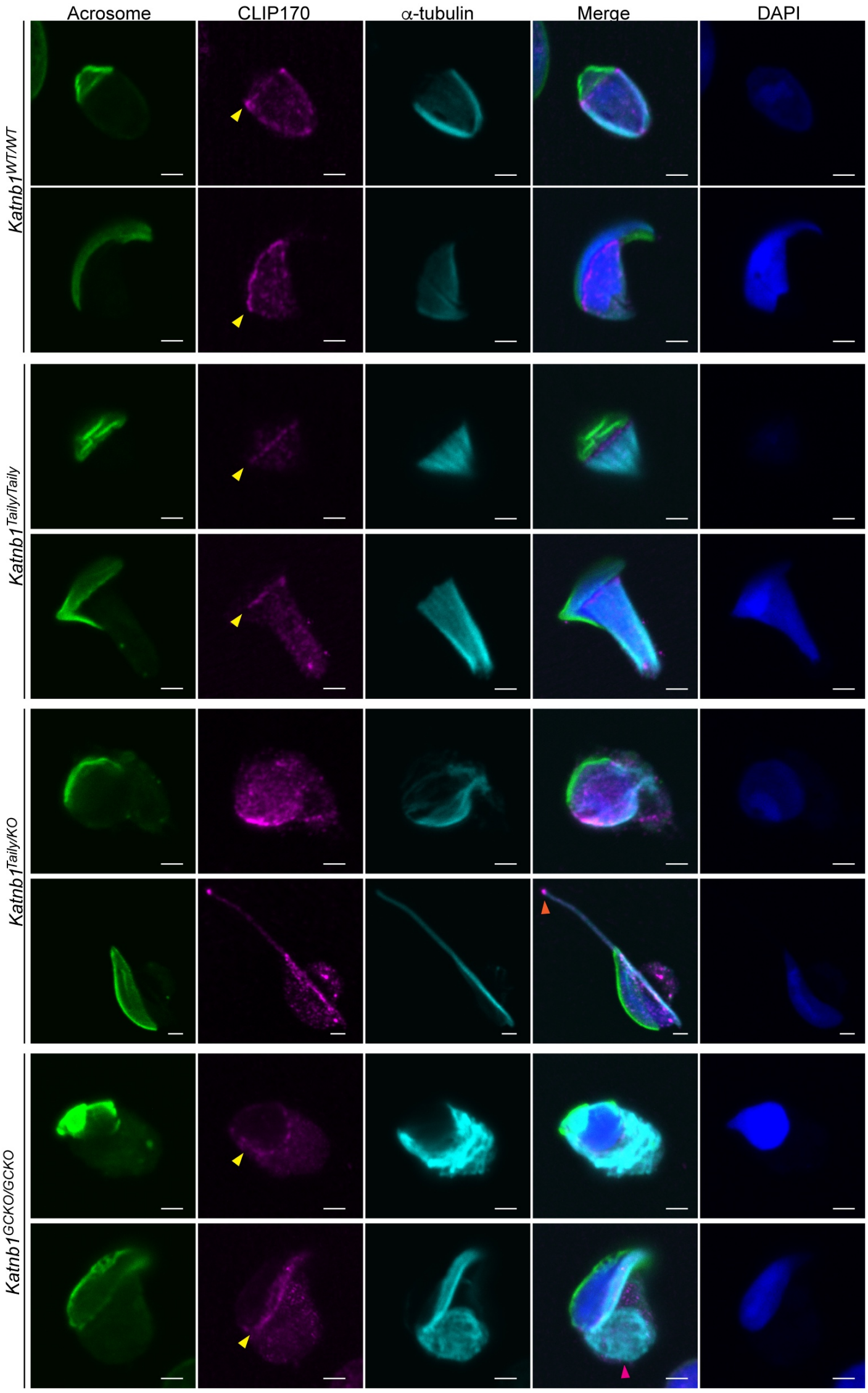
Acrosome
CLIP170
α-tubulin
Merge
DAPI
Katnb1WT/WT
Katnb1Taily/Taily
Katnb1Taily/KO
Katnb1GCKO/GCKO

Fig. S5 Perinuclear ring formation in KATNB1 LOF mice.

CLIP170 (magenta) and α-tubulin (cyan) immunolabelling as a marker of the manchette perinuclear ring/MT plus ends and of the manchette MTs respectively, in *Katnb1*$^{WT/WT}$, *Katnb1*$^{Taily/Taily}$, *Katnb1*$^{Taily/KO}$ and *Katnb1*$^{GCKO/GCKO}$ isolated spermatids. Cells were stained with PNA (green) as a marker of the acrosome and DAPI (blue) to visualise DNA. Yellow arrowheads mark the manchette perinuclear rings which formed in *Katnb1*$^{WT/WT}$, *Katnb1*$^{Taily/Taily}$ and *Katnb1*$^{GCKO/GCKO}$ spermatids. In *Katnb1*$^{Taily/KO}$ MT plus ends were not arranged into a discernible perinuclear ring structure and were instead ectopically oriented and/or located, and were arranged in small clusters (orange arrowhead). Scale bars = 2 μm.

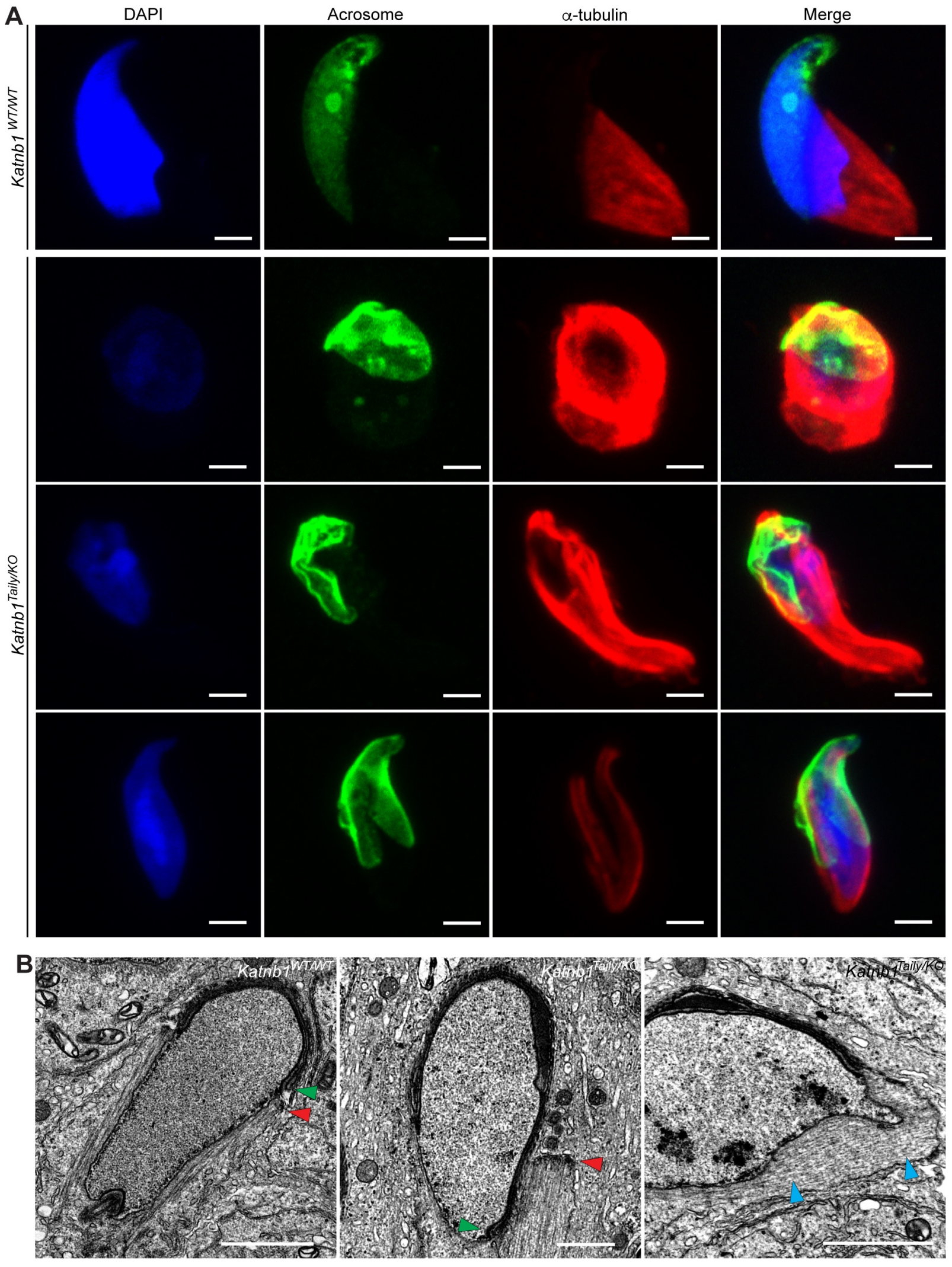

Fig. S6. *Katnb1*$^{Taily/KO}$ spermatids exhibit ectopic manchette-like MTs.

(**A**) α-tubulin immunolabelling (red) as a marker of manchette MTs, in *Katnb1*$^{WT/WT}$ and *Katnb1*$^{Taily/KO}$ isolated spermatids. Cells were counterstained with FITC-PNA (green) as a marker of acrosomes and DAPI (blue) to visualise DNA. Scale bars = 2 μm. (**B**) TEM of *Katnb1*$^{WT/WT}$ and *Katnb1*$^{Taily/KO}$ step 10 spermatids. In *Katnb1*$^{WT/WT}$ mice during sperm head shaping the manchette perinuclear ring (red arrowhead) was always located immediately distal to the leading edge of the acrosome (green arrowhead) and manchette MTs were always oriented in parallel to the long axis of the cell. In *Katnb1*$^{Taily/KO}$ spermatids the perinuclear ring was frequently not observed or ectopic fragments of perinuclear and manchette MTs (red arrowheads) were observed, which were neither situated distal to the acrosome leading edge (green arrowhead) nor associated with the nucleus. In *Katnb1*$^{Taily/KO}$ spermatids manchette-like MTs (blue arrowheads) incorrectly oriented along the long axis of the cell were also frequently observed. Scale bars = 2 μm.

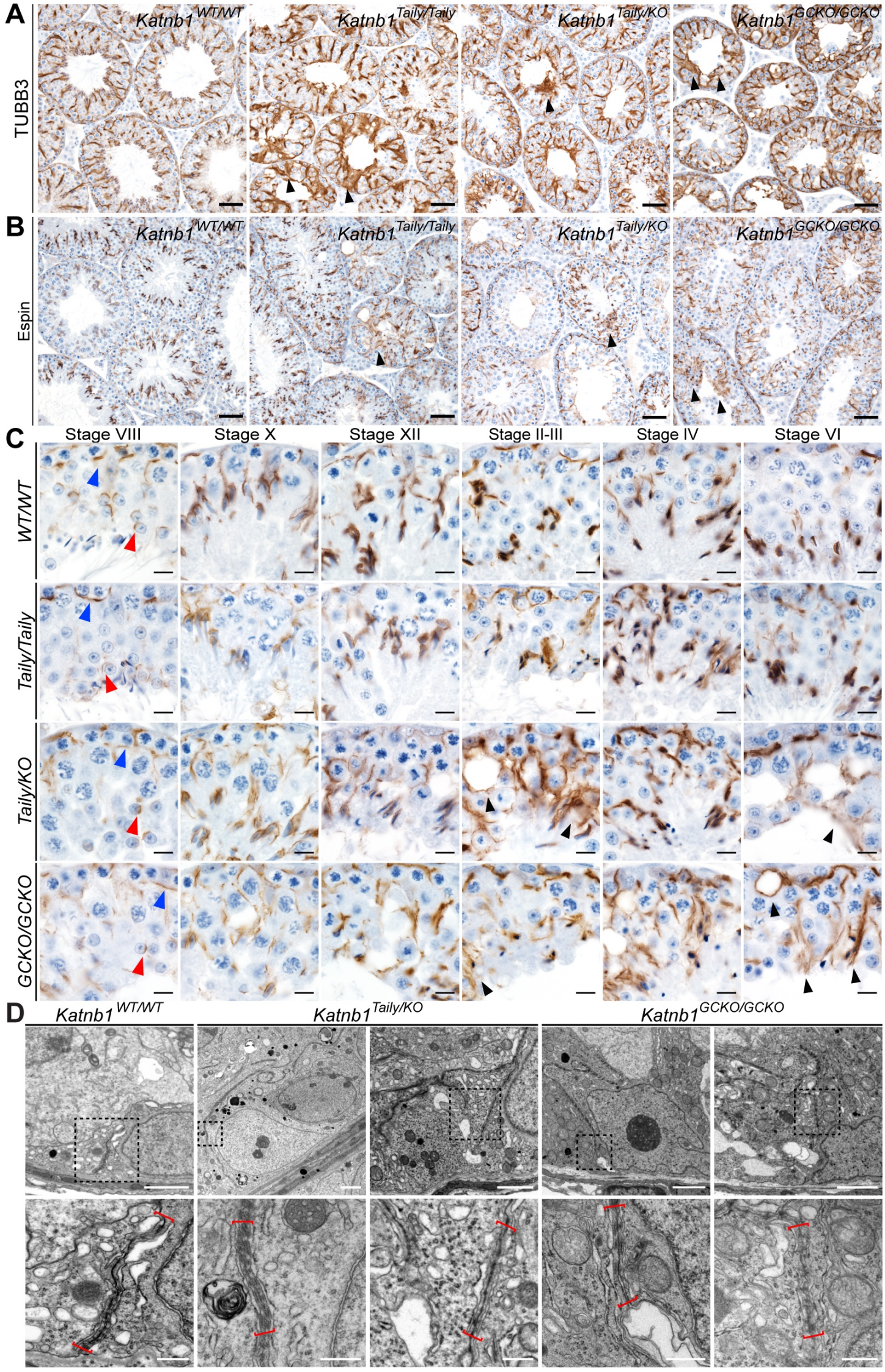

Fig. S7. The Sertoli cell cytoskeleton is disrupted in all three KATNB1 LOF models Testis sections immunolabelled with TUBB3 (**A)** as a marker of Sertoli cell specific MTs and espin (**B,C**) as a marker of ES junctions in KATNB1 LOF mice. TUBB3 immunolabelling (**A**) revealed disorganisation of the Sertoli cell cytoskeleton in *Katnb1*$^{Taily/Taily}$, *Katnb1*$^{Taily/KO}$ and *Katnb1*$^{GCKO/GCKO}$ mice compared to controls. Abnormal enrichment of Sertoli cell MTs (black arrowheads) was observed in areas of *Katnb1*$^{Taily/Taily}$, *Katnb1*$^{Taily/KO}$ and *Katnb1*$^{GCKO/GCKO}$ seminiferous epithelium devoid of germ cells and around pyknotic germ cells. Espin immunolabelling (**B,C)** revealed basal ES junctions (blue arrowheads) were overtly normal in KATNB1 LOF mice compared to controls. Apical ESs formed normally in KATNB1 LOF mice at stage VIII between step 8 spermatids and Sertoli cells (**C**, red arrowheads), however as spermiogenesis progressed ectopic tracts of ES accumulated in disorganised areas of seminiferous epithelium and at sites of germ cell loss (**B,C**, black arrowheads). Scale bars **A**,**B** = 50 μm, **C** = 10 μm. TEM of the basal ES of the blood-testis-barrier in *Katnb1*$^{WT/WT}$, *Katnb1*$^{Taily/KO}$ and *Katnb1*$^{GCKO/GCKO}$ mice (**D**). Lower panels (scalebars = 0.5 μm) correspond to higher magnification images of upper panels (scalebars = 2 μm). Red brackets indicate the basal ES.

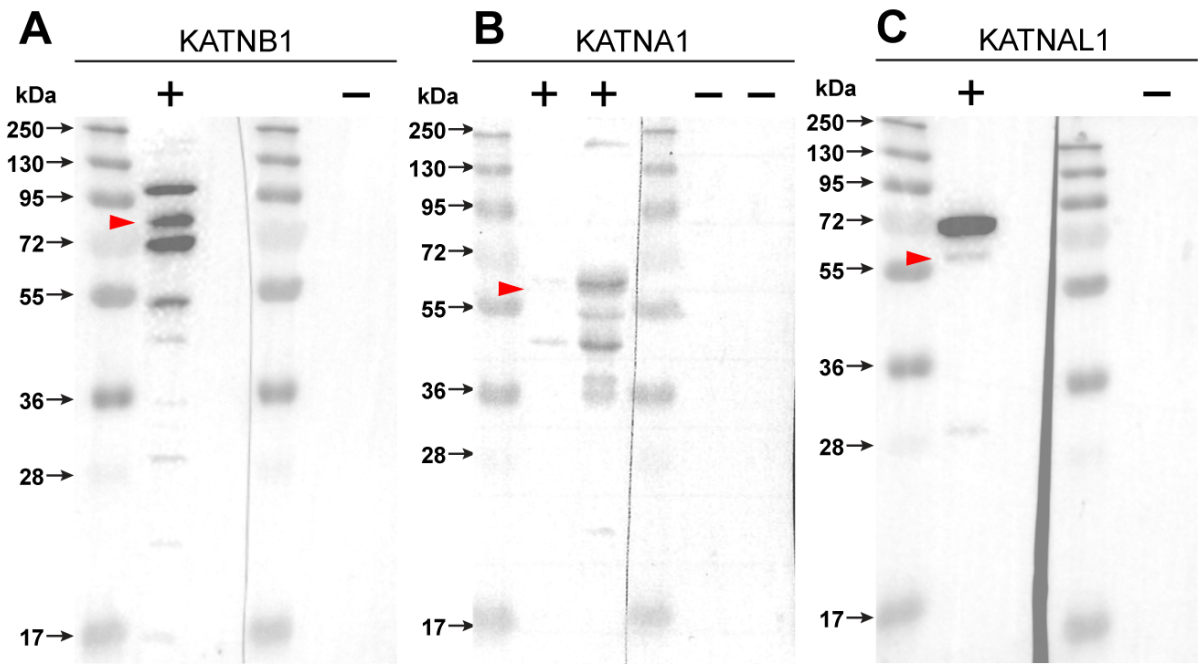

Fig. S8. Validation of the KATNB1, KATNA1 and KATNAL1 antibodies.

Specificity of the KATNB1 (**A**), KATNA1 (**B**) and KATNAL1 (**C**) antibodies was determined by pre-absorption of each with a molar excess of the corresponding immunising peptide prior to immuno-detection on whole adult mouse testes homogenates. Positive control immunoblots for each antibody (+) were conducted in parallel and compared to the pre-absorption controls (-). Red arrowheads indicate the predicted size of the canonical isoform of each protein.